First and second law analyses of nanofluid forced convection in a partially-filled porous channel -The effects of local thermal non-equilibrium and internal heat sources

Craig Dickson [a], Mohsen Torabi [b], Nader Karimi [1, a]

[a] School of Engineering, University of Glasgow, Glasgow G12 8QQ, United Kingdom

[b] The George W. Woodruff School of Mechanical Engineering, Georgia Institute of Technology, Atlanta, GA 30332, USA

Abstract

Generation of entropy and transfer of heat during forced convection of a nanofluid through a partially-filled porous channel are investigated theoretically. The problem includes a fully developed flow in a channel with a central porous insert and under constant heat flux boundary condition. The system is assumed to be under local thermal non-equilibrium and the solid and nanofluid phases can feature internal heat generations. Darcy-Brinkman model of momentum transfer along with the two-equation thermal energy transport and two different fundamental porous-fluid interface models are utilised to analyse the heat transfer problem. Analytical expressions are developed for the temperature fields, Nusselt number and, the local and total entropy generations. The subsequent parametric study reveals the strong influences of the pertinent parameters and the utilised porous-nanofluid interface models. In keeping with others, the results show considerable increases in the Nusselt number with increasing the concentration of nanoparticles. Internal heat generations are demonstrated to have major effects on the heat transfer and entropy generation characterises of the system. Further, the existence of internal heat sources signifies the role of nanoparticles concentration in the thermal and entropic behaviours of the system. It is, also, shown that the choice of the porous-nanofluid interface model can significantly alter the predictions of the local and total entropy generations within the system. This appears to be, particularly, the case at low Biot numbers for which the system is significantly away from the local thermal equilibrium condition.

Keywords: Forced convection in porous media; Nanofluid; Internal heat sources; Entropy generation; Local thermal non-equilibrium;

Nomenclature

a_{sf}	Interfacial area per unit volume of porous media (m^{-1})	*Greek Symbols*	
Bi	Biot number, $\frac{a_{sf} h_{sf} h_0^2}{(1-\varepsilon)k_s}$	μ	Porosity of the porous medium
$c_{nf,p}$	Specific heat of the nanofluid, (J $Kg^{-1}k^{-1}$)	,	Dimensionless temperature
Da	Darcy number, K/h_o^2	$\mu_{nf,eff}$	Viscosity of the nanofluid in porous media (Kg

1 Corresponding author.
E-mails: Nader.Karimi@glasgow.ac.uk (N.Karimi), Torabi_mech@yahoo.com (M. Torabi)

			$m^{-1}s^{1}$)
D_h	Hydraulic diameter of the channel ($4h_0$)	μ_{nf}	Viscosity of nanofluid (Kg $m^{-1}s^{1}$)
h_{sf}	Fluid to solid heat transfer coefficient (W $m^{-2}k^{-1}$)	$Á_{nf}$	Density of nanofluid, (kg/m^3)
h_0	Height of the channel (m)	¾	Constant parameter used in Eq. (43)
h_p	Porous substrate thickness (m)	φ_1	Constant parameter defined by Eq. (54a)
K	Permeability of the porous medium (m^2)	φ_2	Constant parameter defined by Eq. (54b)
k	Ratio of the solid effective thermal conductivity to that of the fluid, $(1-\mu)k_s/(\mu k_{nf})$	φ_3	Constant parameter defined by Eq. (54c)
k_f	Thermal conductivity of the base fluid (W $m^{-1}k^{-1}$)	ω_{nf}	Normalised energy source term in nanofluid defined by Eq. (22i)
k_{nf}	Thermal conductivity of the nanofluid (W $m^{-1}k^{-1}$)	ω_s	Normalised energy source term in fluid defined by Eq. (22j)
k_p	Thermal conductivity of the solid particles in nanofluid (W $m^{-1}k^{-1}$)	ϕ	Volume fraction of the solid particles in the nanofluid
$k_{nf,eff}$	Effective thermal conductivity of the nanofluid, μk_{nf}	*Subscripts*	
k_s	Thermal conductivity of the solid (W $m^{-1}k^{-1}$)	*eff*	Effective property
$k_{s,eff}$	Effective thermal conductivity of the solid, $(1-\mu)k_s$	*f*	Fluid
q	Heat flux (W m^{-2})	f_1	Fluid in the open region
S	Ratio of the porous medium thickness to the channel height, h_p/h_0	f_2	Fluid in the porous medium
S_{nf}	Energy source in nanofluid phase per unit volume (W/m^3)	*nf*	Nanofluid
S_s	Energy source in solid phase per unit volume (W/m^3)	*p*	Porous medium
T	Temperature (K)	*s*	Solid
u	Longitudinal velocity (m/s)	*w*	Wall
$\overline{u}$	Average velocity	interface	The interface between the porous medium and the clear region
u_r	Characteristic velocity, $-\frac{h_0^2}{\mu}\frac{\partial p}{\partial x}$		
U	Dimensionless velocity, u/u_r	*Superscripts*	
$\overline{U}$	Dimensionless average velocity		
x	Longitudinal coordinate (m)	−	Mean value
y	Transverse coordinate (m)	´,´´, ´´´, ´´´´	First, second, third, and forth derivatives with respect to Y
Y	Dimensionless y coordinate, y/h_0		

Z	Constant parameter, $Z = \sqrt{R_u/Da}$

1. Introduction

Since the introduction of nanofluids in 1990's [1] there has been a surge of interest in the applications of nanofluids in heat convection. The subject has already received a significant attention [2, 3] and is growing rapidly [4, 5].The fundamental aspects of heat conduction in nanofluids were discussed by Vadasz [6]. Later, Kakac and Pramuanjaroenkij [7] reviewed the literature on convective heat transfer enhancement by nanofluids. Despite the fact that the use of nanofluids as heat transferring agents is limited to fairly recent past, there already exist sizeable bodies of literature on specialised application areas. For example, applications of nanofluid in solar energy technologies were reviewed by Mahian et al. [8]. Recently, Lomascolo et al. [9] reviewed the experimental analyses on different modes of heat transfer in the media which involve nanofluids. These references all indicate that nanofluids are deemed an attractive option for the highly efficient thermal systems [10] and that the development of various nanofluid thermal systems continues in future [11]. Part of this ongoing effort is devoted to the integration of nanofluids with the existing methods of heat transfer improvement [12]. Inclusion of porous media in fluid conduits sets a well-known example of these methods.

Over the last two decades, the research on fully and partially filled porous channels has been most intensive [13, 14]. Although this area of research is still very active, it is clear that filling the flow conduits with porous materials can significantly enhance the rate of heat transfer with the expense of inducing large pressure drops [13]. Partial filling is known as a solution for this problem [15]. Under partial filling, porous inserts occupy a fraction of the flow volume. A large number of investigations have predicted the rate of heat transfer and pressure drop in the partially-filled porous channels and optimal configurations have been found for various applications, see for example [15, 16, 17]. Replacement of the fluid phase with a nanofluid has also attracted some attention. The general problem of convection in nanofluid saturated porous media has been recently reviewed by Mahdi et al. [12]. Noticeably, a significant fraction of this survey [12] is dedicated to natural and mixed convection. This indicates that only a limited number of studies exists on the forced convection of nanofluids in porous media. A similar point was also made by Nield and Kuznetsov in their recent review of the subject in the latest version of handbook of porous media [18]. Importantly, Nield and Kuznetsov highlighted forced convection of nanofluids through porous media as a research field which deserves immediate attention [18].

For conciseness reasons, here the natural and mixed convection of nanofluids in porous media are not discussed, see Refs. [12, 18] for the reviews of literature on these topics. There are, currently, a very limited number of studies on the forced convection of nanofluids in porous media and these have all appeared in recent years. In a theoretical investigation, Ghazvini and Shokouhmand [19] modelled the problem of nanofluid flow in a row of micro-channels as a flow through porous media. Their analysis involved exploring the influences of particle volume fraction and Brownian–Reynolds number on the temperature distribution and the overall heat transfer coefficient [19]. Further, they examined the effects of different channel aspect ratios and porosities [19]. Hatami and Ganji [20] argued that heat transfer in nanofluid saturated micro-channel heat sinks is analogous to that in porous media. These authors considered the Brownian motion of the nanoparticles and through a

numerical analysis showed that the increase in the volume fraction of particles increases the heat transfer rate of the system [20]. Bachok et al. [21] conducted a numerical study on the flow and heat transfer of nanofluids in a configuration involving rotating porous disks. They used two different models of the effective thermal conductivity and investigated the flow and thermal characteristics of the system [21]. In their numerical work, Maghrebi et al. [22] released the assumption of uniform distribution of nanoparticles in the forced convection of nanofluids through a porous channel. They considered the simultaneous problems of momentum and heat transport along with the transfer of particles by convection and diffusion [22]. Their analyses showed that an increase in Lewis number results in decreasing the local Nusselt number in the porous channel. However, the volume fraction of the nanoparticles appeared to be rather insensitive to the variation in Lewis number [22]. Habibi Matin and Pop [23] investigated nanofluid flow through a fully-filled porous channel. Their investigated configuration included a catalytic reaction occurring on the wall of the channel [23]. These authors took a local equilibrium approach and developed analytical solutions for the velocity, temperature and concentration fields as well as the Nusselt number [23]. In keeping with the previous investigations, Habibi Matin and Pop [23] showed that increasing the volume fraction of nanoparticles results in increasing the rate of heat transfer. The recent analytical studies of Ting et al. [24, 25] under symmetric and asymmetric configurations showed the significance of viscous dissipation effect. These authors [24, 25] demonstrated that ignoring the viscous effects could lead to considerable over-prediction of the rate of heat transfer. The problem of forced convection of heat in a nanofluid saturated porous medium between two parallel plates was investigated by Nield and Kuznetsov [26]. These authors assumed local thermal equilibrium (LTE) between the fluid and solid matrix and derived analytical expressions for Nusselt number by considering the diffusion of nanoparticles [26]. Hatami et al. [27] numerically analysed the flow between counter-rotating disks with porous faces. They considered mixtures of water with a number of metal and metal oxide nanoparticles [27]. Hatami et al., subsequently, conducted an extensive study on the influences of nanoparticle size and type upon the thermal behaviour of the system [27]. The problem of nanofluid flow and heat transfer between rotating porous disks was, further, examined by Hosseini et al. [28]. These authors employed homotopy perturbation method and showed that, in general, increasing the concentration of nanoparticles signifies the Nusselt number. According to the results of Hooseini et al. [28] there is a monotonic and almost linear relationship between the volumetric fraction of nanoparticles and Nusselt number increase. The forced convection of nanofluid in channels partially filled by porous materials has received little attention so far. The numerical work of Servati et al. [29] is one of the few existing studies in the field. These authors investigated the effects of an imposed magnetic field on the forced convection of nanofluid in a partially filled porous channel subject to constant wall temperatures [29]. This study showed that, similar to that obtained in full porous channels, adding nanoparticles to partially-filled porous channels leads to major increases in the rate of heat transfer [29].

It is, now, well established that the performance of thermal systems can be evaluated more comprehensively through a second law analysis [30, 31]. Entropy generation studies have already been conducted on a wide range of thermal systems [31]. The superior thermal conductivity of nanofluids and their slightly enhanced viscosity enables them to influence the flow irreversibility by a significant extent. As a result, there have been a large number of second law analyses of heat transfer in nanofluids, see Refs. [32] and [33] for reviews of literature. Despite the frequency of studies on entropy generation in clear nanofluid conduits, such analyses in porous channels are rather rare. Mahian et al. [33] identified this shortage and recommended paying further attention to

the problem of second law analysis of nanofluid flow and heat transfer in porous media. A second law analysis of nanofluid flow in a configuration including a porous component was put forward by Rashidi et al. [34]. These authors considered the magneto-hydrodynamics of a nanofluid flow in a rotating system with porous disks. They developed numerical solutions for the skin friction factor, Nusselt number and entropy generation rate [34]. The thermodynamic analysis in this work revealed that the surface of the porous disk is a major source of irreversibility. Most recently, Ting et al. [35, 36] analytically examined the thermal characteristics and entropic behaviour of a fully-filled porous channel saturated with nanofluid. Their investigated configuration was subject to fully developed flow and asymmetric thermal boundary conditions [36], and could also feature internal heat generation in the solid phase [35]. These authors applied the local thermal non-equilibrium (LTNE) concept and showed that the addition of nanoparticles reduces the local temperature difference between the solid and fluid phases [35]. It was shown that the existence of internal heat sources in the solid phase majorly affect the system irreversibility. In particular, this study showed that the internal heat generation in the solid phase has destructive effects upon the second law performance of the system [35]. It is important to note that the general problem of convection in porous media with internal heat sources has recently attracted a considerable attention [37, 38, 39]. This is due to the practical applications of this problem in areas such as electronics cooling, chemical and nuclear reactors, solar collectors and fuel cells. Most recently, it has been demonstrated that internal heat sources in either of the solid or fluid phase can significantly modify the temperature fields [40] Nusselt number and entropic behaviour of the system [41].

The preceding review of literature revealed the following points.

- The existing studies on forced convection of nanofluids in porous media are limited and a major fraction of them is devoted to rotating systems. Hence, only a few studies address the problem of forced convection of nanofluids in porous channels [23, 29, 35, 42].
- Given that there exists a large volume of literature on the general subject of forced convection in porous media, the shortage of equivalent studies on nanofluid is most noticeable. As argued by Nield and Kuznetsov [18], there is a serious need for further studies on forced convection of nanofluids in conduits fully or partially filled by porous materials. Further, this problem has been described as an essential and mostly unexplored area of research [33].
- Most existing studies of entropy generation and forced convection of nanofluid through porous media, have assumed LTE. The LTNE analyses of nanofluids in porous media are limited to few very recent investigations [24, 35, 42].
- Nanofluids find direct applications in areas such as electronics cooling, nuclear reactors and solar collectors, in which internal heat generations are unavoidable. Inclusion of internal heat sources in the analysis of porous media has revealed that this could impart substantial effects upon the thermal and entropic behaviours of the system [40, 41]. Nonetheless, with the exception of the recent study of Ting et al. [35], internal source terms have been excluded from the forced convection analyses of nanofluids in porous media.
- Partially-filled porous channels are shown to be an optimal thermo-hydraulic configuration [13, 14]. However, currently little is known about the influences of nanofluid upon the thermal and entropic behaviours of these systems. As a matter of fact, in general, the second law performance of the partially filled systems is not fully understood and research in this area is ongoing [41, 43].

The current study aims at addressing these outstanding issues through a series of theoretical studies. Forced convection of nanofluid on a flow conduit partially-filled by a central porous insert is considered. The system is assumed to be under the LTNE condition and features internal heat generations in both solid and nanofluid phases. The LTE analysis is also performed and compared with the LTNE model. The temperature fields in such system with ordinary fluids has been recently analysed by Karimi et al. [40]. Similar to the analysis in Ref. [40] different porous-fluid interface models [44, 45] are employed to define the thermal boundary conditions. The current study builds upon the work of Karimi et al. [40] and extends that to nanofluids. Most importantly, this work involves Nusselt number and, local and total entropy generation analyses, which were absent in Ref. [40]. It is noted that to the best of the authors' knowledge currently there is no study on the thermodynamics of nanofluid saturated, partially-filled, heat generating porous channels.

2. Analytical analyses

2.1. Problem configuration, assumptions and governing equations

Figure 1 schematically depicts the problem investigated in the present study. A flow of nanofluid moves into a channel in which a porous material is placed at the centre of a two-dimensional channel. The channel walls are subject to a constant heat-flux. The height of the porous insert is h_p and that of the full channel is h_0. Symmetry exists about the centreline of the channel and thus only half of the configuration is analysed. The proceeding analyses involve the following assumptions.

- The porous insert is isotropic and homogeneous.
- The porous system is under LTNE condition.
- The flow is steady, laminar and incompressible and features a uniform distribution of nanoparticles.
- The flow is thermally and hydrodynamically fully developed in all regions.
- Natural convection and radiation heat transfer are not considered here, as gravitational effects are ignored and the emissivity of the material is considered to be negligible. Further, heat generation due to viscous resistance is ignored.
- Thermo-physical properties such as porosity, specific heat and concentration of nanoparticles are constant.
- Heat is generated or consumed uniformly and steadily throughout the nanofluid and solid phases with specified rates.

Given these assumptions, the momentum equation in the clear region reduces to

$$-\frac{\partial p}{\partial x}+\frac{\partial^2 u_{nf}}{\partial y^2}=0. \tag{1}$$

Darcy-Brinkman model is employed to describe the transport of momentum in the porous region,

$$-\frac{\partial p}{\partial x}+\mu_{eff}\frac{\partial^2 u_p}{\partial y^2}-\frac{\mu_{nf}}{K}u_p=0. \tag{2}$$

The energy balance in the clear region is written as

$$\rho_{nf}c_{nf,p}u_{nf}\frac{\partial T_{nf1}}{\partial x}=k_{nf}\frac{\partial^2 T_{nf1}}{\partial y^2}+S_{nf}. \tag{3}$$

Transport of thermal energy for the nanofluid within the porous media reads

$$\rho_{nf} c_{nf,p} u_p \frac{\partial T_{nf2}}{\partial x} = k_{nf,eff} \frac{\partial^2 T_{nf2}}{\partial y^2} + a_{sf} h_{sf} (T_s - T_{nf2}) + S_{nf}, \quad (4)$$

and, the energy equation in the solid phase of the porous region can be written as follows

$$0 = k_{s,eff} \frac{\partial^2 T_s}{\partial y^2} - a_{sf} h_{sf} (T_s - T_{nf2}) + S_s. \quad (5)$$

2.2. Boundary conditions

The momentum equations are subject to the following boundary conditions

$$u_{nf} = 0, \qquad at\ y = h_{0,\#} \quad (6)$$

$$u_f = u_p, \quad \mu_{nf,eff} \frac{\partial u_{nf}}{\partial y} = \mu_{eff} \frac{\partial u_p}{\partial y}, \qquad at\ y = h_{p,\#} \quad (7)$$

$$\frac{\partial u_p}{\partial x} = 0 \qquad at\ y = 0,_{\#} \quad (8)$$

The following boundary conditions apply to the energy equations.

$$k_{nf} \frac{\partial T_{nf1}}{\partial y} = q_w, \qquad at\ y = h_0 \quad (9)$$

$$T_{nf1} = T_{nf2} \qquad at\ y = h_p. \quad (10)$$

$$\frac{\partial T_{nf2}}{\partial y} = \frac{\partial T_s}{\partial y} = 0, \qquad at\ y = 0 \quad (11)$$

Two well established interface models (Model 1A and model 2A of Alazmi and Vafai [45], or Models A and B of Yang and Vafai [46]) are extended to nanofluids. These models describe how heat is distributed between the solid and fluid phases at the porous-fluid interface. Model A assumes that total heat flux is the sum of the conductive heat fluxes of either phase at the interface. That is heat division between the two phases according to their effective thermal conductivities and temperature gradients [40, 46].

$$q_{interface} = k_{nf,eff} \frac{\partial T_f}{\partial y}\Big|_{interface} + k_{s,eff} \frac{\partial T_s}{\partial y}\Big|_{interface} \quad (12a)$$

$$T_{nf}|_{interface} = T_s|_{interface} = T|_{interface} \quad (12b)$$

In Model B, both solid and nanofluid phases are assumed to receive an equal heat flux at the interface, irrespective of their individual thermal conductivities [40, 44, 46].

$$q_{interface} = k_{nf,eff} \frac{\partial T_{nf}}{\partial y}\Big|_{interface} = k_{s,eff} \frac{\partial T_s}{\partial y}\Big|_{interface} \quad (13)$$

In Eqs. (12) and (13) $q_{interface} = k_{nf,eff} \frac{\partial T_{nf1}}{\partial y}\Big|_{y=h_p}$ refers to the heat flux and $T_{\text{interface}}$ refers to the temperature, both at the porous-nanofluid interface. The averaged fluid velocity within the channel is by definition

$$\bar{u} = \frac{1}{h_0}\left[\int_0^{h_p} u_p dy + \int_{h_p}^{h_0} u_{nf} dy\right]. \quad (14)$$

Integrating Eq. (3) through the clear section of the channel and recalling that in the fully developed region $\frac{\partial T_{nf1}}{\partial x} = \frac{\partial T_{nf2}}{\partial x} = \frac{\partial T_{nf}}{\partial x} = \text{const}$, yield

$$\rho_{nf} c_{nf,p} \frac{\partial T_{nf}}{\partial x} \int_{h_p}^{h_0} u_f dy = (q_w - q_{interface}) + \int_{h_p}^{h_0} S_{nf}\, dy. \quad (15)$$

Combining energy Eqs. (4) and (5), integrating over the porous region and applying the interface Model A render

$$\rho_{nf} c_{nf,p} \frac{\partial T_{nf}}{\partial x} \int_0^{h_p} u_p dy = q_{interface} + \int_0^{h_p} (S_{nf} + S_s) dy . \tag{16}$$

.

Combining Eqs. (15) and (16), then implementing Eq. (14) reveals

$$\rho_{nf} c_{nf,p} \frac{\partial T_{nf}}{\partial x}\Big|_{Model\ A} = \frac{q_w}{h_0\ \bar{u}} + \left(\int_0^{h_0} S_{nf}\ dy + \int_0^{h_p} S_s\ dy \right) \frac{1}{h_0\ \bar{u}}. \tag{17}$$

The heat flux at the porous-nanofluid interface according to Model A can be defined by substituting Eq. (17) into Eq. (16)

$$\begin{aligned} \frac{q_{interface}}{q_w}\Big|_{Model\ A} &= \frac{1}{h_0\ \bar{u}} \int_0^{h_p} u_p dy \\ &+ \frac{1}{q_w} \left[\frac{1}{h_0\ \bar{u}} \left(\int_0^{h_0} S_{nf}\ dy + \int_0^{h_p} S_s\ dy \right) \int_0^{h_p} u_p dy - \int_0^{h_p} (S_{nf} + S_s) dy \right]. \end{aligned} \tag{18}$$

The same procedure can be followed to attain the heat flux at the interface according to Model B. Combining Eqs. (4) and (5), integrating over the porous insert and applying Model B boundary condition Eq. (13) results in

$$\rho_{nf} c_{nf,p} \frac{\partial T_{nf}}{\partial x} \int_0^{h_p} u_p dy = 2\ q_{interface} + \int_0^{h_p} (S_{nf} + S_s) dy. \tag{19}$$

Combining Eqs. (15) and (19), then using Eq. (14) yields,

$$\rho_{nf} c_{nf,p} \frac{\partial T_{nf}}{\partial x}\Big|_{Model\ B} = \frac{1}{h_0\ \bar{u}} (q_w + q_{interface}) + \left(\int_0^{h_0} S_{nf}\ dy + \int_0^{h_p} S_s\ dy \right) \frac{1}{h_0\ \bar{u}}. \tag{20}$$

Substituting Eq. (20) into Eq. (19) renders the following prediction of the heat flux at the interface according to Model B.

$$\begin{aligned} \frac{q_{interface}}{q_w}\Big|_{Model\ B} &= \frac{\int_0^{h_p} u_p dy}{2\ h_0\ \bar{u} - \int_0^{h_p} u_p dy} \\ &- \frac{h_0\ \bar{u}}{2\ h_0\ \bar{u} - \int_0^{h_0} u_p dy} \left[\frac{1}{q_w} \int_0^{h_p} (S_{nf} + S_s) dy - \frac{1}{q_w} \frac{\int_0^{h_p} u_p dy}{h_0\ \bar{u}} \left(\int_0^{h_0} S_{nf}\ dy + \int_0^{h_p} S_s\ dy \right) \right]. \end{aligned} \tag{21}$$

.

2.3. Normalisations and velocity profiles

Dimensionless variables are introduced to normalise the governing equations and boundary conditions.

$$\theta|_{Model\ A} = \frac{k_{s,eff}(T - T_{interface})}{q_w h_0} \tag{22a}$$

$$\theta|_{Model\ B} = \frac{k_{s,eff}(T - T_{s,interface})}{q_w h_0} \tag{22b}$$

$$\gamma = \frac{q_{interface}}{q_w} \tag{22c}$$

$$k = \frac{k_{s,eff}}{k_{nf,eff}} \tag{22d}$$

$$Bi = \frac{h_{sf} a_{sf} {h_0}^2}{k_{s,eff}} \tag{22e}$$

$$Y = \frac{y}{h_0} \tag{22f}$$

$$S = \frac{h_p}{h_0} \tag{22g}$$

$$U = \frac{u}{u_r} \tag{22h}$$

$$R_k = \frac{k_{nf}}{k_f} = 1 + \frac{3\phi\left(\frac{k_p}{k_f}-1\right)}{\left(\frac{k_p}{k_f}+2\right)-\phi\left(\frac{k_p}{k_f}-1\right)} \tag{22i}$$

$$R_\mu = \frac{\mu_{nf}}{\mu_f} = \frac{1}{1-\phi^{2.5}} \tag{22j}$$

The characteristic velocity is defined as $u_r = -\frac{{h_0}^2}{\mu_{nf}}\frac{\partial p}{\partial x}$. The Biot number (*Bi*) provides a simple representation of the heat transfer resistance inside and at the surface of a body. More specifically, *Bi* is the ratio of solid phase conduction resistance over the actual heat exchanged between the fluid and solid phases. Further, *k* is a ratio of the effective thermal conductivities of the solid phase and nanofluid phases. Equations (22i) and (22j) introduce relations between thermal conductivity and viscosity of the base fluid and nanofluid. These well-established models are discussed by Torabi et al. [32], and were developed by Maxwell-Garnetts and Brinkman respectively [47, 48].

Using dimensionless parameters in the momentum equations, the following normalised relations for the velocity fields are obtained

$$0 = 1 + R_\mu \frac{\partial^2 U_f}{\partial y^2}, \qquad S < Y < 1,\# \tag{23a}$$

$$0 = 1 + \frac{\partial^2 U_p}{\partial y^2} - \frac{R_\mu}{Da} U_p, \qquad 0 < Y < S,\# \tag{23b}$$

with the following boundary conditions

$$U_{nf} = 0, \qquad at\ Y = 1, \tag{23c}$$

$$U_{nf} = U_p, \quad R_\mu \frac{\partial U_{nf}}{\partial Y} = \frac{\partial U_p}{\partial Y}, \qquad at\ Y = S, \tag{23d}$$

$$\frac{\partial U_p}{\partial Y} = 0 \qquad at\ Y = 0. \tag{23e}$$

The velocity in the clear fluid region becomes

$$U_{nf}(Y) = \left(-\frac{1}{2}Y^2 + AY + B\right)\frac{1}{R_\mu}, \tag{24}$$

where

$$A = S + \frac{Z\ sinh(ZS)(S - 0.5(1+S^2) + Da)}{Z(S-1)sinh(ZS) - R_\mu cosh(ZS)}, \tag{25a}$$

$$B = \frac{1}{2} - A. \tag{25b}$$

Within the porous insert, we have

$$U_p(Y) = C\ cosh(ZS) + \frac{Da}{R_\mu}, \tag{26}$$

$$C = \frac{1}{Z\ sinh(Z\ S)}\ (A - S). \tag{27}$$

Taking Eqs. (24) and (26) and the dimensionless variables in Eq. (22), the dimensionless average velocity in Eq. (14) is written as,

$$\bar{U} = S\frac{Da}{R_\mu} + \frac{C}{Z}sinh(ZS) + \frac{1}{R_\mu}\left[-\frac{1}{6}(1-S^3) + \frac{1}{2}A(1-S^2) + B(1-S)\right]. \tag{28}$$

Expressions for A, B and C are provided by Eqs. (25a), (25b) and (27) and $Z = \sqrt{R_u/Da}$. The normalised velocity fields are now used in the heat flux at the porous interface, and further to produce the temperature fields from the energy equations. By making Eq. (18) dimensionless, we derive an expression for the heat flux at porous-nanofluid interface under Model A

$$\gamma|_{Model\ A} = \frac{1}{\overline{U}} \int_0^S U_p dY + \left[\frac{1}{\overline{U}}\left(\int_0^1 \omega_{nf}\, dY + \int_0^S \omega_s\, dy\right)\int_0^S U_p dy - \int_0^S (\omega_{nf} + \omega_s) dY\right]. \tag{29}$$

Substituting Eqs. (26) and (28) into (29) reads

$$\gamma|_{Model\ A} = \frac{\frac{C}{Z} sinh(ZS) + \frac{Da}{R_\mu} S}{\frac{Da}{R_\mu} S + \frac{C}{Z}\, sinh(ZS) + \frac{1}{R_\mu}\left[-\frac{1}{6}(1-S^3) + \frac{1}{2}A(1-S^2) + B(1-S)\right]}\left[1 + (\omega_{nf} + S\omega_s)\right] - S(\omega_{nf} + \omega_s). \tag{30}$$

The non-dimensional form of Eq. (21) can be used to derive an expression for the heat flux at the interface according to Model B:

$$\gamma|_{Model\ B} = \frac{\int_0^S U_p dY}{2\,\overline{U} - \int_0^S U_p dY} - \frac{\overline{U}}{2\,\overline{U} - \int_0^S U_p dY}\left[\int_0^S (\omega_f + \omega_s) dY - \frac{\int_0^S U_p dY}{\overline{U}}\left(\int_0^1 \omega_f\, dY + \int_0^S \omega_s\, dy\right)\right]. \tag{31}$$

Through substituting Eq. (26) into (28), Eq. (31) can be written as follows

$$\begin{aligned}
&\gamma|_{Model\ B} \\
&= \frac{\frac{C}{Z} sinh(ZS) + \frac{Da}{R_\mu} S}{2\left(\frac{Da}{R_\mu} S + \frac{C}{Z}\, sinh(ZS) + \frac{1}{R_\mu}\left[-\frac{1}{6}(1-S^3) + \frac{1}{2}A(1-S^2) + B(1-S)\right]\right) - \frac{C}{Z} sinh(ZS) + \frac{Da}{R_\mu} S} \\
&- \frac{\frac{Da}{R_\mu} S + \frac{C}{Z}\, sinh(ZS) + \frac{1}{R_\mu}\left[-\frac{1}{6}(1-S^3) + \frac{1}{2}A(1-S^2) + B(1-S)\right]}{2\left(\frac{Da}{R_\mu} S + \frac{C}{Z}\, sinh(ZS) + \frac{1}{R_\mu}\left[-\frac{1}{6}(1-S^3) + \frac{1}{2}A(1-S^2) + B(1-S)\right]\right) - \frac{C}{Z} sinh(ZS) + \frac{Da}{R_\mu} S} \times \\
&\left[S(\omega_{nf} + \omega_s) - \frac{\frac{C}{Z} sinh(ZS) + \frac{Da}{R_\mu} S}{\frac{Da}{R_\mu} S + \frac{C}{Z}\, sinh(ZS) + \frac{1}{R_\mu}\left[-\frac{1}{6}(1-S^3) + \frac{1}{2}A(1-S^2) + B(1-S)\right]}(\omega_{nf} + S\omega_s)\right].
\end{aligned} \tag{32}$$

2.4 Solid and fluid temperature fields

2.4.1. Model A predictions of the temperature fields

By employing the non-dimensional parameters in Eq. (22), Eqs. (3), (4) and (5) can be used to produce non-dimensional energy equations for the channel. This turns the energy equation in the clear region to

$$\varepsilon k \frac{U_{nf}}{\overline{U}}(1 + \omega_{nf} + S\omega_s) = R_k \theta''_{nf1}(Y) + \omega_{nf}. \tag{33}$$

For the fluid within the porous region, the energy equation expands to

$$\frac{U_p}{\overline{U}}(1 + \omega_{nf} + S\omega_s) = \frac{R_k}{k}\theta''_{nf2}(Y) + Bi\big(\theta_s(Y) - \theta_{nf2}(Y)\big) + \omega_{nf}. \tag{34}$$

Finally, transport of energy in the solid phase can be written as

$$0 = \theta''_s(Y) - Bi\left(\theta_s(Y) - \theta_{nf2}(Y)\right) + \omega_s. \tag{35}$$

The boundary conditions applied to these equations can be also written in dimensionless form as follows,

$$R_k\theta'_{nf1}(Y) = \varepsilon k, \tag{36}$$

$$\theta_s(S) = \theta_{nf1}(S) = \theta_{nf2}(S) = 0,\# \tag{37a}$$

$$\theta'_s(0) = \theta'_{nf2}(0) = 0. \tag{37b}$$

By taking the second derivative with respect to *Y*, the coupled differential Eqs. (34) and (35) are converted to the following fourth order ordinary differential equations

$$\theta''''_{nf2}(Y) - Bi\left(1+\frac{k}{R_k}\right)\theta''_{nf2}(Y) = \frac{k}{R_k\bar{U}}\left(1+\omega_{nf}+S\omega_s\right)\left[-BiU_p(Y)+U''_p(Y)\right] + Bi\frac{k}{R_k}\left(\omega_{nf}+\omega_s\right), \tag{38}$$

$$\theta''''_s(Y) - Bi\left(1+\frac{k}{R_k}\right)\theta''_s(Y) = -\frac{k}{R_k\bar{U}}\left[-BiU_p(Y)\left(1+\omega_{nf}+S\omega_s\right)\right] + Bi\frac{k}{R_k}\left(\omega_{nf}+\omega_s\right). \tag{39}$$

Taking the second and third derivatives of θ_{f2} and θ_s at *Y*=0 and *Y*=*S* and, substituting Eqs. (37a) and (37b) into Eqs. (34) and (35) reveal

$$\begin{aligned} &R_k\theta''_{nf2}(S) = k\frac{U_p(S)}{\bar{U}}\left(1+\omega_{nf}+S\omega_s\right) - k\omega_{nf}, && \theta''_s(S) = -\omega_s, \\ &\theta'''_{nf2}(0) = 0, && \theta''_s(0) = 0. \end{aligned} \tag{40}$$

By integrating Eq. (33), we obtain Model A prediction of the temperature field in the clear region. This reads

$$\begin{aligned} \theta_{nf1}(Y)\big|_{Model\ A} = \frac{\varepsilon k}{\bar{U}R_\mu R_k}\Bigg\{&\left(1+\omega_{nf}+S\omega_s\right)\left(-\frac{Y^4}{24}+A\frac{Y^3}{6}+B\frac{Y^2}{2}\right) \\ &+\left(1+\omega_{nf}+S\omega_s\right)\left(\frac{1}{6}-\frac{A}{2}-B\right)Y - \left(1+\omega_{nf}+S\omega_s\right)\left(-\frac{S^4}{24}+A\frac{S^3}{6}+B\frac{S^2}{2}\right) \\ &+S\left(1+\omega_{nf}+S\omega_s\right)\left(-\frac{1}{6}+\frac{A}{2}+B\right) + \bar{U}R_\mu(Y-S) \\ &+\omega_{nf}\frac{\bar{U}R_\mu}{\varepsilon k}\left[(Y-S)-\frac{1}{2}(Y^2-S^2)\right]\Bigg\}. \end{aligned} \tag{41}$$

.

Temperature fields in the porous region are developed by solving Eqs. (38) and (39) through implementing the boundary conditions given by Eqs. (37) and (40). This provides the following expressions for the temperature distributions inside the porous region for the nanofluid and solid phases respectively.

$$\begin{aligned} \theta_{nf2}(Y)\big|_{Model\ A} = \frac{k}{\bar{U}R_\mu}\Bigg\{&\frac{C(Z^2-Bi)\left(1+\omega_{nf}+S\omega_s\right)[cosh(ZY)-\cosh(ZS)(1+Z^2\xi)]}{Z^2(Z^2-\Gamma^2)} \\ &+\left(\frac{\frac{Bi}{R_k}\left(Da\left(1+\omega_{nf}+S\omega_s\right)-\bar{U}R_\mu(\omega_{nf}+\omega_s)\right)}{\Gamma^2}\right)\left(-\xi+\frac{Y^2}{2}-\frac{S^2}{2}\right) \\ &+U_p(S)\left(1+\omega_{nf}+S\omega_s\right)\xi-\bar{U}\omega_{nf}\xi\Bigg\}, \end{aligned} \tag{42}$$

$$\begin{aligned} \theta_s(Y)\big|_{Model\ A} = -Bi\frac{k}{\bar{U}R_\mu}\Bigg\{&\frac{C\left(1+\omega_{nf}+S\omega_s\right)[cosh(ZY)-\cosh(ZS)(1+Z^2\xi)]}{Z^2(Z^2-\Gamma^2)} \\ &-\frac{Da}{\Gamma^2R_\mu}\left(1+\omega_{nf}+S\omega_s\right)\left(-\xi+\frac{Y^2}{2}-\frac{S^2}{2}\right)+\frac{\bar{U}}{\Gamma^2}\left(\omega_{nf}+\omega_s\right)\Bigg\}-\omega_{nf}\xi, \end{aligned} \tag{43}$$

where $\Gamma = \sqrt{Bi(1+k)}$ and $\xi = \left(\frac{cosh(\Gamma Y)}{\cosh(\Gamma S)} - 1\right) / \Gamma^2$.

2.4.2. Model B predictions of the temperature fields

Solving Eqs. (3), (4) and (5) and substituting the boundary condition provided in Eq. (22b) results in the energy equations for the solid and nanofluid regions according to Model B. The energy equation in the clear region can be expressed as

$$\frac{U_f}{\bar{U}}\left(1+\gamma+\omega_{nf}+S\omega_s\right) = \frac{R_k}{\varepsilon\, k}\theta''_{nf1}(Y) + \omega_{nf}. \tag{44}$$

Transport of energy for the fluid phase within the porous insert is reduced to,

$$\frac{U_p}{\bar{U}}\left(1+\gamma+\omega_{nf}+S\omega_s\right) = \frac{R_k}{k}\theta''_{nf2}(Y) + Bi\left(\theta_s(Y)-\theta_{nf2}(Y)\right) + \omega_{nf}. \tag{45}$$

Finally, the solid phase energy equation within the porous media becomes

$$0 = \theta''_s(Y) - Bi\left(\theta_s(Y)-\theta_{nf2}(Y)\right) + \omega_s. \tag{46}$$

The boundary conditions corresponding to these equations are

$$R_k\theta'_{nf1}(1) = \varepsilon\, k, \tag{47a}$$

$$\theta_{nf1}(S) = \theta_{nf2}(S), \tag{47b}$$

$$\theta'_{nf2}(0) = \theta'_S(0) = 0, \tag{47c}$$

$$R_k\theta'_{nf2}(S) = \gamma\, k, \tag{47d}$$

$$\theta'_s(S) = \gamma, \tag{47e}$$

$$\theta''_s(S) + Bi\;\theta_{nf2}(S) + \omega_{nf} = 0, \tag{47f}$$

$$\theta_s(s) = 0. \tag{47g}$$

Eqs. (45) and (46) are decoupled by taking the second derivative with respect to *Y*.

$$\begin{aligned}\theta''''_{nf2}(Y) - Bi\left(1+\frac{k}{R_k}\right)\theta''_{nf2}(Y) \\ = \frac{k}{R_k\bar{U}}\left(1+\gamma+\omega_{nf}+S\omega_s\right)\left[-BiU_p(Y)+U''_p(Y)\right] + Bi\frac{k}{R_k}(\omega_{nf}+\omega_s)\end{aligned} \tag{48}$$

$$\theta''''_s(Y) - Bi\left(1+\tfrac{k}{R_k}\right)\theta''_s(Y) = -Bi\tfrac{k}{R_k\bar{U}}\left(1+\gamma+\omega_{nf}+S\omega_s\right)U_p(Y) + Bi\tfrac{k}{R_k}(\omega_{nf}+\omega_s). \tag{49}$$

The second and third derivatives of θ_{nf2} and θ_S at *Y*=0 are evaluated through the application of Eq. (47). This results in

$$\theta''''_{nf2}(Y) = R_k\, k\,\tfrac{U'_p(0)}{\bar{U}} = 0, \tag{50a}$$

$$\theta'''_s(Y) = 0. \tag{50b}$$

By solving the ordinary differential equation presented in Eq. (44), we obtain Model B prediction in the clear region, where

$$\theta_{nf1}(Y)\big|_{\,Model\;B} = \frac{\varepsilon k}{\bar{U}R_\mu R_k}\left[\left(1+\gamma+\omega_{nf}+S\omega_s\right)\left(-\frac{Y^4}{24}+A\frac{Y^3}{6}+B\frac{Y^2}{2}\right)\right] - \frac{\epsilon\, k}{2R_k}\omega_{nf} + O_1Y + O_2, \tag{51a}$$

$$O_1 = \frac{\varepsilon k}{\bar{U}R_\mu R_k}\left[\left(1+\gamma+\omega_{nf}+S\omega_s\right)\left(-\frac{1}{6}+\frac{A}{2}+B\right)\right] + \frac{\epsilon\, k}{R_k}\omega_{nf} + \frac{\epsilon\, k}{R_k}, \tag{51b}$$

$$O_2 = \theta_{nf2}(S) - \frac{\varepsilon k}{\bar{U} R_\mu R_k}\left[\left(1+\gamma+\omega_{nf}+S\omega_s\right)\left(-\frac{S^4}{24}+A\frac{S^3}{6}+B\frac{S^2}{2}\right)\right] - \frac{\epsilon\, k}{2R_k}\omega_{nf}S^2 - O_1 S. \tag{51c}$$

Solving Eqs. (48) and (49) with conditions given in Eqs. (47) and (50) reveals the temperature distributions in the porous region:

$$\theta_{nf2}(Y)\big|_{Model\ B} = \frac{\varphi_1}{\Gamma^2}\cosh(\Gamma Y) + \left[\frac{Bi\frac{k}{R_k}(\omega_{nf}+\omega_s)}{\Gamma^2} + \frac{\frac{k}{\bar{U}}\frac{R_\mu}{R_k}\left(1+\gamma+\omega_{nf}+S\omega_s\right)Bi\ Da}{\Gamma^2}\right]\left(\frac{Y^2}{2}\right) + \frac{k}{\bar{U}R_k}\left(\frac{C(Z^2-Bi)\left(1+\gamma+\omega_{nf}+S\omega_s\right)}{Z^2(Z^2-\Gamma^2)}\right)\cosh(ZY) + \varphi_3, \tag{52}$$

$$\theta_s(Y)\big|_{Model\ B} = \frac{\varphi_2}{\Gamma^2}[cosh(\Gamma Y) - \cosh(\Gamma S)] + \left[-\frac{Bi\frac{k}{R_k}(\omega_{nf}+\omega_s)}{\Gamma^2} + \frac{\frac{k}{\bar{U}}\frac{1}{R_k R_\mu}\left(1+\gamma+\omega_{nf}+S\omega_s\right)Bi\ Da}{\Gamma^2}\right]\left(\frac{Y^2}{2}-\frac{S^2}{2}\right) - \frac{k}{\bar{U}R_k}\left(\frac{C\ Bi\left(1+\gamma+\omega_f+S\omega_s\right)}{Z^2(Z^2-\Gamma^2)}\right)[cosh(ZY) - \cosh(ZS)], \tag{53}$$

where,

$$\varphi_1 = \frac{\Gamma}{\sinh(\Gamma S)}\left[\frac{k\,\gamma}{R_k} - \frac{\frac{k}{\bar{U}}\frac{R_\mu}{R_k}\left(1+\gamma+\omega_{nf}+S\omega_s\right)Bi\ Da}{\Gamma^2}S + \frac{Bi\frac{k}{R_k}(\omega_{nf}+\omega_s)}{\Gamma^2}S - \frac{k}{\bar{U}R_k}\left(\frac{C(Z^2-Bi)\left(1+\gamma+\omega_{nf}+S\omega_s\right)}{Z^2(Z^2-\Gamma^2)}\right)\sinh(ZS)\right], \tag{54a}$$

$$\varphi_2 = \frac{\Gamma}{sinh(\Gamma S)}\left[\gamma - \frac{\frac{k}{\bar{U}}\frac{1}{R_k R_\mu}\left(1+\gamma+\omega_{nf}+S\omega_s\right)Bi\ Da}{\Gamma^2}S + \frac{Bi\frac{k}{R_k}(\omega_{nf}+\omega_s)}{\Gamma^2}S + \frac{Bi\ k}{\bar{U}R_k}\left(\frac{C\left(1+\gamma+\omega_{nf}+S\omega_s\right)}{Z^2(Z^2-\Gamma^2)}\right)sinh(ZS)\right], \tag{54b}$$

$$\phi_3 = Cosh(\Gamma S)\left[\frac{\varphi_1}{\Gamma^2}-\frac{\varphi_2}{Bi}\right] + \left[\frac{\frac{k}{\bar{U}}\frac{R_u}{R_k}\left(1+\gamma+\omega_{nf}+S\omega_s\right)Bi\ Da}{\Gamma^2} + \frac{Bi\frac{k}{R_k}(\omega_{nf}+\omega_s)}{\Gamma^2}\right]\left(-\frac{1}{Bi}-\frac{S^2}{2}\right) + \frac{Bi\ k}{\bar{U}R_k}\left(\frac{C\left(1+\gamma+\omega_{nf}+S\omega_s\right)}{Z^2(Z^2-\Gamma^2)}\right)\cosh(ZS) - \frac{\omega_{nf}}{Bi}. \tag{54c}$$

2.4.3. LTE solution

By taking the uncoupled energy equations within the porous region, the system can be solved for the LTE case. Combining Eqs. (34) and (35) gives

$$\frac{R_k}{k}\Theta''_{nf2}(Y) + \Theta''_s(Y) + \omega_{nf} + \omega_s = \frac{U_p}{\bar{U}}\left(1+\omega_{nf}+S\omega_s\right). \tag{55}$$

Under LTE condition $\Theta_{nf2} = \Theta_s = \theta$. Therefore, Eq. (55) reduces to

$$\left(\frac{R_k}{k}+1\right)\theta'' = \frac{U_p}{\bar{U}}\left(1+\omega_{nf}+S\omega_s\right)-(\omega_{nf}+\omega_s). \tag{56}$$

This one-equation model is subject to the following boundary conditions

$$\frac{\partial\theta}{\partial Y}(y=0)=0, \qquad \theta(S)=\theta_{nf1}(S). \tag{57}$$

Integrating Eq. (56) and using boundary conditions given in Eq. (57), the full LTE temperature field can be expressed as

$$\theta_p(Y)\big|_{LTE} = \frac{k}{R_k+k}\left\{\frac{1}{\bar{U}}\left(\frac{C[cosh(ZY)-\cosh(ZS)]}{Z^2}+\frac{Da}{R_\mu}(Y^2-S^2)\right)\left(1+\omega_{nf}+S\omega_s\right)-\frac{1}{2}(\omega_{nf}+\omega_s)(Y^2-S^2)\right\}. \tag{58}$$

2.5 Nusselt number

Nusselt Number at the channel wall for S<1 (Partial filling) is given by Roshenow and Hartnett [49].

$$Nu = \frac{q_w D_h}{k_{nf}(T_w - T_m)}. \tag{59}$$

For the fully developed channel [14]:

$$Nu = \frac{q_w D_h}{k_{nf,eff}(T_w - T_m)}. \tag{60}$$

D_h is the hydraulic diameter of the channel, and equal to $4h_0$. Equations (58) and (59) can be written with non-dimensional parameters. For S<1:

$$Nu = \frac{4\varepsilon k}{(\theta_w - \theta_m)}. \tag{61}$$

For S=1:

$$Nu = \frac{4\varepsilon}{(\theta_w - \theta_m)}, \tag{62}$$

where,

$$\theta_w = \theta_{nf1}\big|_{Y=1}. \tag{63}$$

θ_m is the non-dimensional mean temperature, and is defined as:

$$\theta_m = \frac{\int_0^S U_p\theta_{nf2}dy + \int_S^1 U_{nf}\theta_{nf1}dy}{\bar{U}}. \tag{64}$$

Eqs. (61) and (64) include massive algebraic manipulations. Hence, Wolfram Mathematica was used to conduct the algebraic work. Analytical expressions were developed for Nusselt number under Models A and B. Nonetheless, since these expressions are lengthy and cumbersome, they are not shown here.

2.6 Entropy generation

The equations for the local entropy generation rate [41, 43] within the three components of the system can be written as follows

$$\dot{S}'''\big|_{nf2} = \frac{k_{nf,eff}}{T_{nf2}^2}\left(\left(\frac{dT_{nf2}}{dx}\right)^2 + \left(\frac{dT_{nf2}}{dy}\right)^2\right) + \frac{h_{sf}a_{sf}(T_s - Tn_{f2})^2}{T_s T_{nf2}} + \frac{\mu_{nf}}{kT_{nf2}}u_p^2 + \frac{\mu_{nf,eff}}{T_{nf2}}\left(\frac{du_p}{dy}\right)^2 \qquad 0 < y < h_{p,} \qquad (65)$$

$$\dot{S}'''\big|_{s} = \frac{k_{s,eff}}{T_s^2}\left(\left(\frac{dT_s}{dx}\right)^2 + \left(\frac{dT_s}{dy}\right)^2\right) + \frac{h_{sf}a_{sf}(T_s - T_{nf2})^2}{T_s T_{nf2}} \qquad 0 < y < h_{p,} \qquad (66)$$

$$\dot{S}'''\big|_{nf1} = \frac{k_{nf}}{T_{nf1}^2}\left(\left(\frac{dT_{nf1}}{dx}\right)^2 + \left(\frac{dT_{nf1}}{dy}\right)^2\right) + \frac{\mu_{nf}}{kT_{nf1}}u_{nf}^2 \qquad h_p < y < h_{o,} \qquad (67)$$

It is essential to note that, as discussed in Ref. [41], the internal heat sources do not explicitly appear in the entropy formulations given by Eqs. (65)-(67), and their effects are represented by the temeprature fields. The dimensionless local volumetric entropy generation rate $N_s = \frac{\dot{S}^m h_0^2}{k_{s,eff}}$ for all parts of the system is given by the followings.

$$N_s|_{nf2} = \frac{Rk}{k(\theta_{nf2}+B)^2}\left(\left(\frac{(1-\gamma)+\int_S^1 \omega_{nf}dY}{\frac{Pe}{k}\int_S^1 U_{nf}dY}\right)^2 + \left(\frac{d\theta_{nf2}}{dY}\right)^2\right) + \frac{Bi(\theta_s - \theta_{nf2})^2}{(\theta_s+B)(\theta_{nf2}+B)} + \frac{R_\mu Br U_p^2}{Da(\theta_{nf2}+B)} + \frac{R_\mu Br}{\varepsilon(\theta_{nf2}+B)}\left(\frac{dU_p}{dY}\right)^2 \qquad 0 < Y < S, \qquad (68)$$

$$N_s|_{s} = \frac{1}{k(\theta_s+B)^2}\left(\left(\frac{(1-\gamma)+\int_S^1 \omega_{nf}dY}{\frac{Pe}{k}\int_S^1 U_{nf}dY}\right)^2 + \left(\frac{d\theta_s}{dY}\right)^2\right) + \frac{Bi(\theta_s - \theta_{nf2})^2}{(\theta_s+B)(\theta_{nf2}+B)} \qquad 0 < Y < S, \qquad (69)$$

$$N_s|_{f1} = \frac{Rk}{k\varepsilon(\theta_{nf1}+B)^2}\left(\left(\frac{(1-\gamma)+\int_S^1 \omega_{nf}dY}{\frac{Pe}{k}\int_S^1 U_{nf}dY}\right)^2 + \left(\frac{d\theta_{nf1}}{dY}\right)^2\right) + \frac{BrU_{nf1}^2}{Da(\theta_{nf1}+B)} \qquad S < Y < 1, \qquad (70)$$

where for Model A, $B = \frac{T_S k_{s,eff}}{q_w h_0}$, for Model B, $B = \frac{T_{s,int} k_{s,eff}}{q_w h_0}$ and $Pe = \frac{h_0 \rho_{nf} c_{p,nf} u_r}{k_{f,eff}}$. Finally, the dimensionless volumetric averaged entropy generation rate is given by

$$N_t = \int_0^1 N_s dY. \qquad (71)$$

3. Results and discussion

In this section expressions derived in section 2 are used to analyse the temperature fields, Nusselt number and entropy generation rates of the system. First, a validation of the presented mathematical manipulations is put forward. Then, two main cases are analysed, which firstly include a channel with internal heat source through the solid phase of the porous medium. Typical examples of this case can be readily found in electronics cooling and nuclear reactors. In the second case heat generation exists only in the fluid phase. Chemical reactors are the main representation of this group of problems. Unless otherwise stated, to calculate the results of this section, the following values of the parameters have been used:#$B = 10,\ \varepsilon = 0.5, Pe = 10,\ Br = 10$.

3.1. Validation

It is noted that in the limit of zero concentration of the nanoparticles (i.e. ϕ=0) the analytical expressions, derived in section 2, for the velocity and temperature fields reduce to those of Ref. [40]. Figure 2 shows that in this limit and in the absence of internal heat generations (i.e, $\omega_{nf} = \omega_s = 0$), the predicted Nusselt numbers are identical to those calculated previously by Ref. [50] for ordinary fluids. Further, in the presence of thermal

source terms the temperature fields predicted by the current derivations for ϕ=0 appear to be identical to those of Ref. [40]. This series of evidence confirm the validity of the current work.

3.2. Temperature and Nusselt number

Figures 3-6 show the nanofluid temperature distributions inside the porous medium and the clear region for varying nanoparticles concentration. In Fig. 3 the internal heat generations are set to zero and nanofluid temperature has been calculated under interface models A and B, while the value of thermal conductivity and Biot number vary. This figure clearly shows the negligible variations of the nanofluid temperature inside the porous region with changes in nanoparticle concentrations. However, the nanofluid temperature profiles within the clear region feature a more noticeable change and show a reduced value at higher concentrations of nanoparticles. Introduction of an internal heat source in the solid phase (Fig. 4) or within the nanofluid phase (Fig. 5) leads to considerable modifications of the temperature profiles. First, unlike those with no internal heat generation (see Fig. 3) these cases show noticeable changes in nanofluid temperature within the porous region. This is particularly true for the cases with low thermal conductivity ratio shown in Fig. 4. Second, compared to Fig. 3, in Fig. 4 the sensitivity of the nanofluid temperature fields to Biot number has significantly increased. This is such that increasing the Biot number from 0.1 to 10 in Fig. 4 results in change of the sign of nanofluid dimensionless temperature. Further, the absolute value of the dimensionless temperature grows by an order of magnitude. It should be noted that changes in the sign of the dimensionless temperatures, as a result of modifications in the Biot number and thermal conductivity ratio, have been previously reported in heat generating porous media [40]. The influence of variations in the heat generation intensity upon the nanofluid temperature is depicted in Fig. 6. Expectedly, increasing the solid internal heat generation substantiates the dimensionless temperature of the nanofluid. This figure, further, represents a mathematical artefact of Models A and B. Model A predicts identical interface temperatures for varying values of ω_s. However, these values are significantly different under Model B and consequently a point of equal nanofluid temperatures appears within the porous medium (see Fig. 6b).

It has been previously reported that changing the internal heat generations inside partially-filled porous channels can produce 'thermal peculiarities' [40]. Yang and Vafai [44] showed that bifurcation of the temperature gradient on the porous-fluid interface activates a new mechanism, in which heat is exchanged from the hot phase first to the interface, then from the interface to the cold phase. This occurs when the signs of the solid and fluid temperature gradients at the interface are opposite of each other. It is essential to understand under which situations a porous system bifurcates, as occurrence of bifurcation highly complicates the behaviour of the system. In mathematical terms, the parameter Σ is used to evaluate heat flux bifurcation, in which $\Sigma = \frac{\theta'_{nf2}(Y)|_{\text{Model A}}}{\theta'_{s}(Y)|_{\text{Model A}}}$ [40]. If $\Sigma < 0$, the temperature gradient at the interface has bifurcated. As discussed by Yang and Vafai [44], such bifurcation only occurs under Model A. This is because Model B automatically equates the signs of the heat fluxes. Figure 7 shows maps of *Bi*-*k* over which the sign of Σ has been calculated for various combinations of ω_f and ω_s. Figures 7b and 7c indicate that changes in nanoparticle concentration can have considerable influences upon heat flux bifurcation. For instance, for a given value of *k* in Fig. 7b increasing the nanoparticle concentration widens the bifurcation area and results in the occurrence of bifurcation at higher values of *Bi*. It is interesting to note that the extent of this influence appears to be strongly dependent

upon the values of ω_{nf} and ω_s. This is such that in some cases (see Fig. 7d) changing the concentration of the nanoparticles hardly modifies the bifurcation map. It follows that for any combination of the internal heat sources the bifurcation map should be constructed separately. The analytical solution developed in section 2 will be instrumental for this purpose.

Figures 8 and 9 show the effects of nanoparticles concentration, porous insert thickness and interface models on the Nusselt number for different values of internal heat sources. These internal heat sources are set to zero in Fig. 8a, b. It is clear from this figure that adding nanoparticles to the base fluid has a very noticeable impact on the Nusselt number. An increase of more than 15% is observed in Nusselt number in the non-heat generating cases. Under Model A, when the porous thickness is close to the height of the channel a local minimum point appears for all investigated nanofluid volume fractions (see Fig. 8a). A similar behaviour has been observed in the previous studies of this configuration considering ordinary fluids [50]. Similar to the previously reported results for ordinary fluids [50], the values of Nusselt number are heavily dependent upon the choice of the interface model. It is, further, important to note that the increase in Nusselt number appears to be proportional with the concentration of the particles in all cases investigated in Fig. 8. However, the extent of the improvements in Nusselt number is strongly dependent on the thickness of the porous insert. Importantly, the maximum enhancement of Nusselt number by nanoparticles appears to be around the maximum *Nu* established by variation in the porous insert thickness. Addition of heat sources to the solid phase in Figs. 8c and d leads to a significant increase in Nusselt number. Further, Figs. 8c and d clearly show that for heat generating cases the difference between *Nu* predictions of the two interface models are significantly different. However, the relative increase in *Nu* by adding nanoparticles remains more and less similar to the non-heat generating case. In Fig 9 Nusselt number of the case with heat generating nanofluid is examined. This indicates a qualitative similarity to those of Figs. 8c and d with solid phase heat generation. Nonetheless, a close inspection of Figs. 8 and 9 reveals that heat generation in nanofluid under Model A increases *Nu* with respect to the corresponding case with heat generating solid (Fig. 8c). However, the opposite trend applies to Model B predictions of the Nusselt number.

3.3. Local and total entropy generation

Figures 10 and 11 show the local entropy generations in the presence of the internal heat generation in the solid phase. A simple comparison between Figs. 10 and 11 reveals that the value of the local entropy generation is dominated by the thermal conductivity ratio. An increase in this parameter leads to significant growth in the local entropy generations in both porous and clear regions. Further, similar to that observed in the temperature distributions, substantial changes in the *Bi* under Model A imparts relatively small modifications on the local entropy generation rate in the channel. However, in keeping with the temperature behaviour under Model B, Biot number can have more pronounced impacts on the value of the local entropy generation rate. Furthermore, introduction of internal heat sources leads to some important features. First, compared to non-heat generating cases (not shown here) the magnitudes of entropy generations for the heat generating cases are larger. This behaviour is similar to that previously reported in other partially-filled, porous channel configurations with the internal heat generations and ordinary fluids [41]. Second, in Figs. 10 and 11 the influences of interface models upon the local entropy generation become more noticeable. For instance, a comparison between Figs. 10a and 10c shows that while all other parameters are the same, there is a significant difference between the local entropy predictions of Models A and B. The same trend is observed in Fig. 11 when the value of thermal conductivity ratio has changed. Evidently, the observed difference between the calculated local entropy

generations under the two models is strongly *Bi* dependent and diminishes at higher *Bi*. This can be understood by considering the fact that, in general, by increasing *Bi* the deviation of the system from LTE decreases [40], [41]. It follows that predictions of the two models should approach each other at higher *Bi* and become identical in the limit of very large *Bi*. Previous studies on ordinary fluids have confirmed the validity of this argument [40, 50, 51].

Figure 12 shows the local entropy generation through the channel for different values of internal heat generation in the solid phase and at high value of Bi. It is clear from this figure that increasing the intensity of the internal heat generation in the solid phase of the system signifies the local entropy generation rate. The general trend in this figure has been observed in other heat generating porous systems [41]. Nonetheless, it is interesting to note that the rate of increase in the local entropy generation with respect to the solid heat generation is strongly nonlinear. This is such that while by increasing ω_s from 0.2 to 2 the values of N_S almost doubles, further increase in ω_s to 20 magnifies N_S by an order of magnitude. This effects appears on both solid and nanofluid phases. Further, Fig. 12 shows that as the intensity of the internal heat generation increases its influence upon the irreversibilities in the nanofluid phase grows. These clearly indicate the importance of including internal heat generations in the entropic analysis of nanofluid flow in porous media.

Figure 13 shows the effects of variations in *Bi* on the total entropy generation rate under interface Models A and B. Both heat generating and non-heat generating cases are examined in this figure. As expected, the total entropy generated in heat generating cases is much higher in comparison with their non-heat generating analogues. Further, the total entropy generation directly correlates with the concentration of nanoparticles. It is noted that similar conclusions have been made in a recent analysis of entropy generation in fully-filled porous channels [36]. Furthermore, in keeping with the earlier discussions, this figure shows that comparing with Model A, the total entropy generations under Model B are larger and also feature a higher sensitivity to the *Bi*. The latter is particularly the case at lower Biot numbers where this parameter has more pronounced effects. Under both investigated interface models and at higher values of *Bi* the rate of change in the total entropy production slows down. As already discussed, this can be attributed to the dominance of the LTNE in the low Biot number. Within the considered range of *Bi* in Fig. 13, total entropy generation under Model B remains *Bi* dependent. However, it becomes almost indifferent to the *Bi* when Model A is in place.

Figures 14-18 have been devoted to the effects of pertinent parameters on the total entropy generation rate and its minimisation. Hence, wherever it is possible, the entropy generation minimisation (EGM) of the system is performed and the optimal values of parameters are reported. The effect of porous thickness on the total entropy generation rate within the channel has been examined in Fig. 14. This figure shows that by increasing the thickness of the porous insert and regardless of the internal heat generations and nanoparticle concentration, the total entropy generation first slightly decreases, reaches a minimum value and then starts to increase. The minimum value for the total entropy generation occurs at $S\sim 0.4$, when internal heat generations are set to zero (see Figs. 14a and c). However, when internal heat generation in solid phase of the porous material is set to 2 (Figs. 14b and d) thinner porous material is needed to achieve the EGM of the system. This value is $S\sim 0.32$ for Fig. 14b and $S\sim 0.35$ for Fig. 14d. The total entropy generation increases considerably between S~ 0.6 and 0.7 and, any increase of the porous insert thickness beyond S~ 0.7 results in very significant increases of the total entropy generation. Further, the distinctions between different nanoparticle concentrations become more apparent at higher thicknesses of the porous insert. Nonetheless, with the exception of the values of *S* close to

unity the difference between the total entropy generations under various nanoparticle concentrations is practically negligible. A comparison between the Nusselt numbers results in Figs. 8 and 9 and those of the total entropy generation in Fig. 14, reveals two important aspects of design optimisation in the system under investigation. Figures 8 and 9 show that the Nusselt number generally reaches its maximum value in the range of S~ 0.7 and 0.8. Yet, the minimal total entropy generation is around S~0.4. Hence, in this problem there exists a difference between the first and second law optimal solutions. Differences in the optimal solutions from different viewpoints have been reported previously in partially-filled porous systems [41] and, it is the specific application area that determines the final choice.

Figure 15 depicts the effects of the intensity of the internal heat generations upon the total entropy generation rate of the system. Positive and negative heat generations in both nanofluid and solid phases are analysed under the two interface models. This figure clearly shows that signifying the internal heat generation intensifies the difference between the total entropy generations calculated for varying concentrations of nanoparticles. There appears to be a growing difference between the ordinary fluid and nanofluid entropic behaviours for finite values of internal heat generation. Further, this figure shows that the total entropy generation initially starts to decrease under negative internal heat sources (endothermicity). However, the trend changes at an extremum point, which can be considered as an EGM case of the system, and entropy generation increases with further intensification of the endothermicity in either of the solid or nanofluid phase. The exact values of ω_s and ω_f at the extreme point depend upon the system parameters and interface model. Nonetheless, the general behaviour remains qualitatively the same for all the investigated cases.

Figures 16-18 can be interpreted similar to Fig. 15 and therefore they are discussed briefly. These figures show the total entropy generation rate versus internal heat generation parameters for various values of pertinent parameters such as Biot number (Fig. 16), thermal conductivity ratio (Fig. 17) and Peclet number (*Pe*) (Fig. 18). Figure 16 shows that different values of *Bi* may not significantly impact the total entropy generation rate. Unlike *Bi*, the thermal conductivity ratio can influence the total entropy generation rate rather drastically (see Fig. 17). Since *Pe* has a substantial effect on the total entropy generation rate, a logarithmic scale has been used in the vertical axis of Fig. 18. It is observed that, when a high value for the internal heat generation/absorption is used, increasing *Pe* form 5 to 10 substantially decreases the total entropy generation rate.

In closing, it is worth mentioning that the engineering applications of this work can be categorised into two major groups. The first is on heat transfer analyses, wherein the main objective is to find the temperature distributions and Nusselt numbers. In particular, the outcomes of this work are applicable to thermal analysis of chemical and nuclear reactors, in which strong internal heat generations are unavoidable. For similar reason, the current work is equally relevant to the field of electronics cooling. The results presented in section 3.2 showed internal heat generation can leave significant effects upon the thermal behaviour of the system. Thus, inclusion of internal heat sources is a real necessity for conduction of representative thermal analysis. The second main family of applications is on thermodynamics analyses and EGM. If the former is the case, the analyses provided here can be used for optimising the cooling parameters of the system. If the latter is desired, the total entropy generation analyses can be employed in an EGM analysis of the system to achieve less exergy destruction.

7. Conclusions

The problems of forced convection of heat and entropy generation in nanofluid flow through a channel partially filled by a porous insert were investigated theoretically. The composite system could include internal heat generations and was under constant heat flux boundary conditions. The LTNE condition was assumed and analytical expressions were developed for the temperature fields, Nusselt number and, local and total entropy generations. Two commonly used interface models (Models A and B of Vafai and his co-worker [46]) were employed to describe the thermal boundary conditions at porous-nanofluid interface. The LTE solution of the temperature field was, further, developed. An extensive parametric study was, subsequently, conducted. The main results of this study can be summarised as follows.

- In the absence of the internal heat generations the influence of nanoparticles on the fluid temperature inside the porous insert was relatively weak. However, this becomes more noticeable in the clear part and particularly in the region close to the channel's walls.
- Introduction of the internal heat generations highly signifies the temperature differences between nanofluids with different concentrations of nanoparticles in both porous and clear regions.
- Nano-particles appeared to be able to affect the heat flux bifurcation. However, the extent of this effect was found to be strongly dependent upon the internal heat sources.
- Addition of nanoparticles was observed to increase the Nusselt number up to more than 15% for both non-heat generating and heat generating cases. Yet, as the previous studies on the ordinary fluids have shown, the Nusselt number predictions were highly affected by the choice of the interface model.
- Variations in the nanoparticle concentration had a considerable effect on the local entropy generations in the nanofluid phase. However, its effect on the entropy generation in the solid phase was almost negligible.
- It was observed that the presence of the internal heat generations highly signifies the dependency of the predicted local entropy generations upon the interface model.
- It was shown that the total entropy generation is strongly Peclect number and conductivity ratio dependent and varies significantly with changes in the internal heat generations.

Overall, the analyses presented in this paper highlighted the importance of interface models as the key element dominating the thermal and entropic behaviours of the system. The current results showed that the addition of internal heat generations intensifies the differences between the thermal characteristics of the system using ordinary and nanofluids. This, in turn, substantiates the importance of interface models in the LTNE analyses of heat generating porous-nanofluids systems.

References

[1] S. Chol, Enhancing thermal conductivity of fluids with nanoparticles, vol. 231, ASME-Publications-Fed, 1995, pp. 99-106.

[2] R. B. Schoch, J. Han and P. Renaud, "Transport phanomena in nanofluids," *Reviews of Modern Physics* , vol. 80, no. 3, p. 839, 2008.

[3] X.-Q. Wang and A. S. Mujumdar, "Heat transfer characteristics of nanofluids: a review," *International journal of thermal sciences* , vol. 46, no. 1, pp. 1-19, 2007.

[4] L. B. Godson, D. Raja, M. Lal and S. Wongwises, "Enhancement of heat transfer using nanofluids—an overview," *Renewable and Sustainable Energy Reviews,* vol. 14, no. 2, pp. 629-

641, 2010.

[5] E. Efstathios and S. Michaelides, Nanofluidics- Thermodynamic and Transport Properties, Switzerland: Springer International Publishing, 2014.

[6] P. Vadasz, "Heat conduction in nanofluid suspensions," *Journal of Heat Transfer,* vol. 128, no. 5, pp. 465-477, 2006.

[7] S. Kakac and A. Pramuanjaroenkij, "Review of convective heat transfer enhancement with nanofluids," *International Journal of Heat and Mass Transfer,* vol. 52, no. 13, pp. 3187-3196, 2009.

[8] O. Mahian, A. Kainifar, S. A. Kalogirou, I. Pop and S. Wongwises, "A review of the applications of nanofluids in solar energy," *International Journal of Heat and Mass Transfer,* vol. 57, no. 2, pp. 582-594, 2013.

[9] M. Lomascolo, G. Colangelo, M. Milanese and A. De Risi, "Review of heat transfer in nanofluids: Conductive, convective and radiative experimental results," *Renewable and Sustainable Energy Reviews ,* vol. 43, pp. 1182-1198, 2015.

[10] W. Daungthongsuk and S. Wongwises, "A critical review of convective heat transfer of nanofluids," *Renewable and Sustainable Energy Reviews ,* vol. 11, no. 5, pp. 797-817, 2007.

[11] J. Sarkar, P. Gosh and A. Adil, "A review on hybrid nanofluids: Recent research, development and applications," *Renewable and Sustainable Energy Reviews,* vol. 43, pp. 164-177, 2015.

[12] R. A. Mahdi, H. Mohammed, K. Munisamy and N. Saeid, "Review of convection heat transfer and fluid flow in porous media with nanofluid," *Renewable and Sustainable Energy Reviews,* vol. 41, pp. 715-734, 2015.

[13] D. A. Nield and A. Bejan, Convection in Porous Media, Springer, 2013.

[14] M. Kavainy, Principles of heat transfer in porous media, Springer Science & Business Media, 2012.

[15] E. Ucar, M. Mobedi and I. Pop, "Effect of an inserted porous layer located at a wall of a parallel plate channel on forced convection heat transfer," *Transport in porous media,* vol. 98, no. 1, pp. 35-57, 2013.

[16] O. Cekmer, M. Mobedi, B. Ozerdem and I. Pop, "Fully developed forced convection in a parallel plate channel with a centered porous layer," *Transport in porous media,* vol. 93, no. 1, pp. 179-201, 2012.

[17] M. Nimvari, M. Maerefat and M. El-Hossaini, "Numerical simulation of turbulent flow and heat transfer in a channel partially filled with a porous media," *International Journal of Thermal Sciences,* vol. 60, pp. 131-141, 2012.

[18] K. Vafai, Handbook of porous media, third edition, CRC Press, 2015.

[19] M. Ghazvini and H. Shokouhmand, "Investigation of a nanofluid-cooled microchannel heat sink using fin and porous media approaches," *Energy conversion and management,* vol. 50, no. 9, pp. 2373-2380, 2009.

[20] M. Hatami and D. Ganji, "Thermal and flow analysis of microchannel heat sink (MCHS) cooled by Cu–water nanofluid using porous media approach and least square method," *Energy Conversion and management ,* vol. 78, pp. 347-358, 2014.

[21] N. Bachok, A. Ishak and I. Pop, "Flow and heat transfer over a rotating porous disk in a nanofluid," *Physica B: Condensed Matter,* vol. 406, no. 9, pp. 1767-1772, 2011.

[22] M. J. Maghrebi, M. Nazari and T. Armaghani, "Forced convection heat transfer of nanofluids in a porous channel," *Transport in porous media,* vol. 93, no. 3, pp. 401-413, 2012.

[23] M. Habibi Matin and I. Pop, "Forced convection heat and mass transfer flow of a nanofluid through a porous channel with a first order chemical reaction on the wall," *International Communications in Heat and Mass Transfer,* vol. 46, pp. 134-141, 2013.

[24] T. W. Ting, , Y. M. Hung and N. Guo, "Viscous dissipative forced convection in thermal non-equilibrium nanofluid-saturated porous media embedded in microchannels," *International Communications in Heat and Mass Transfer,* vol. 57, pp. 309-318, 2014.

[25] T. W. Ting, Y. M. Hung and N. Guo, "Viscous dissipative nanofluid convection in asymmetrically heated porous microchannels with solid-phase heat generation," *International Communications in Heat and Mass Transfer* , vol. 68, pp. 236-247, 2015.

[26] D. Nield and A. Kuznetsov, "Forced convection in a parallel-plate channel occupied by a nanofluid or a porous medium saturated by a nanofluid," *International Journal of Heat and Mass Transfer,* vol. 70, pp. 430-433, 2014.

[27] M. Hatami, M. Sheikholeslami and D. Ganji, "Laminar flow and heat transfer of nanofluid between contracting and rotating disks by least square method," *Powder Technology,* vol. 253, pp. 769-779, 2014.

[28] Hosseini, E. Mohammadian, M. Shirvani, S. Mirzababaei and F. Shakeri Aski, "Thermal analysis of rotating system with porous plate using nanofluid.," *Powder Technology,* vol. 254, pp. 563-571, 2014.

[29] A. Servati, . K. Javaherdeh and H. R. Ashorynejad, "Magnetic field effects on force convection flow of a nanofluid in a channel partially filled with porous media using Lattice Boltzmann Method.," *Advanced Powder Technology* , vol. 25, no. 2, pp. 566-675, 2014.

[30] M. Torabi, K. Zhang, N. Karimi, G. P. Peterson, "Entropy generation in thermal systems with solid structures-a concise review" *International Journal of Heat and Mass Transfer,* vol. 97, pp.917-931, 2016.

[31] M. Torabi, G.P. Peterson, M. Torabi, N. Karimi, "A thermodynamic analysis of forced convection through porous media using pore scale modeling", *International Journal of Heat and mass Transfer,* vol. 99, pp. 303-316, 2016.

[32] M. Torabi, K. Zhang and S. Mahmud, "Temperature and Entropy Generation Analyses Between and Inside Rotating Cylinders Using Copper–Water Nanofluid," *Journal of Heat Transfer,* vol. 137, no. 5, p. 051701, 2015.

[33] O. Mahian, A. Kianifar, C. Kleinstreuer, A.-N. Moh'd A, I. Pop, A. Z. Sahin and S. Wongwises, "A review of entropy generation in nanofluid flow," *International Journal of Heat and Mass Transfer,* vol. 65, pp. 514-532, 2013.

[34] M. M. Rashidi, S. Abelman and N. F. Mehr, "Entropy generation in steady MHD flow due to a rotating porous disk in a nanofluid.," *International Journal of Heat and Mass Transfer,* vol. 62, pp. 515-525, 2013.

[35] T. W. Ting, Y. M. Hung and N. Guo, "Entropy generation of viscous dissipative nanofluid convection in asymmetrically heated porous microchannels with solid-phase heat generation.," *Energy Conversion and Management* , vol. 105, pp. 731-745, 2015.

[36] T. W. Ting, Y. M. Hung and N. Guo, "Entropy generation of viscous dissipative nanofluid flow in thermal non-equilibrium porous media embedded in microchannels," *International Journal of Heat and Mass Transfer,* vol. 81, pp. 862-877, 2015.

[37] G. Chen, C. Tso and Y. M. Hung, "Field synergy principle analysis on fully developed forced convection in porous medium with uniform heat generation.," *International Communications in Heat and Mass Transfer,* vol. 38, no. 9, pp. 1247-1252, 2011.

[38] K. Zheng, Q. Sun and M. Ni, "Local Non-Equilibrium Thermal Effects in Solid Oxide Fuel Cells with Various Fuels," vol. 1, no. 1, pp. 35-41, 2013.

[39] S. Mahjoob and K. Vafai, "Analysis of bioheat transport through a dual layer biological media," *Journal of Heat Transfer,* vol. 132, no. 3, p. 031101, 2010.

[40] N. Karimi, D. Agbo, A. T. Khan and P. L. Younger, "On the effects of exothermicity and endothermicity upon the temperature fields in a partially-filled porous channel," *International Journal of Thermal Sciences,* vol. 96, pp. 128-148, 2015.

[41] M. Torabi, N. Karimi and K. Zang, "Heat transfer and second law analyses of forced convection in a channel partially filled by porous media and featuring internal heat sources," *Energy,* vol. 93, pp. 106-127, 2015.

[42] T. Armaghani, A. J. Chamkha, M. Maghrebi and M. Nazari, "Numerical analysis of a nanofluid forced convection in a porous channel: A new heat flux model in LTNE condition," *Journal of Porous Media*, vol. 17, no. 7, pp. 637-646, 2014.

[43] M. Torabi, K. Zang, G. Yang, Y. Wang and P. Wu, "Heat transfer and entropy generation analyses in a channel partially filled with porous media using local thermal non-equilibrium model," *Energy*, vol. 82, pp. 922-938, 2015.

[44] K. Yang and K. Vafai, "Analysis of heat flux bifurcation inside porous media incorporating inertial and dispersion effects - an exact solution," *International Journal of Heat and Mass Transfer*, vol. 70, pp. 875-891, 2014.

[45] B. Alazmi and K. Vafai, "Analysis of variants within the porous media transport models," *Journal of Heat Transfer*, vol. 122, no. 2, pp. 303-326, 2000.

[46] S. Mahjoob and K. Vafai, "Analytical characterization and production of an isothermal surface for biological and electronic applications," *International Journal of Heat and Mass Transfer*, vol. 52, no. 5, pp. 1608-1618, 2009.

[47] M. Sheikholeslami, M. Bandpy, M. Ellahi, R. Hassan and S. Soleimani, "Effects of MHD on Cu-Water Nanofluid Flow and Heat Transfer by Means of CVFEM," *Journal of Magnetism and Magnetic Materials*, vol. 349, pp. 188-200, 2014.

[48] M. Sheikholeslami, D. Ganji and H. Ashorynejad, "Investigation of Squeezing Unsteady Nanofluid Flow using ADM," *Powder Technology*, vol. 239, pp. 259-265, 2013.

[49] W. Roshenow and J. Hartnett, Handbook of Heat Transfer, Third ed., New York: McGraw- Hill, 1998.

[50] Y. Mahmoudi, N. Karimi and K. Mazaheri, "Analytical investigation of heat transfer enhancement in a channel partially filled with a porous material under local thermal non-equilibrium condition: effects of different thermal boundary conditions at the porous-fluid interface," *International Journal of Heat and Mass Transfer*, vol. 70, pp. 875-891, 2014.

[51] N. Karimi, Y. Mahmoudi, K. Mazaheri, "Temperature fields in a channel partially-filled with a porous material under local thermal non-equilibrium condition-an exact solution", *Proceedings of the Institution of Mechanical Engineering, Part C, Journal of Mechanical Engineering Science*, vol. 228(15), pp. 2778-2789, 2014.

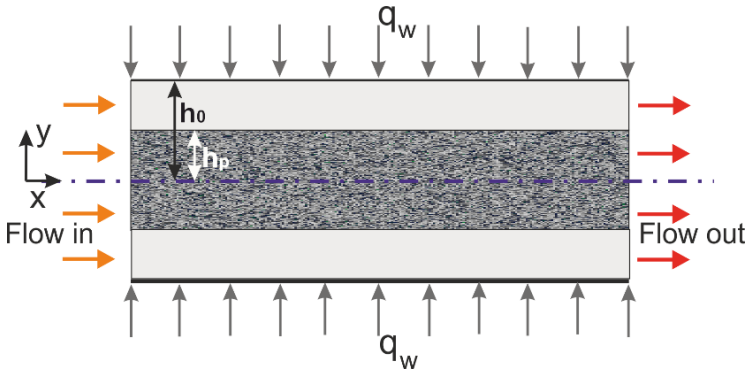

Fig. 1. Configuration of the channel partially filled with a porous material.

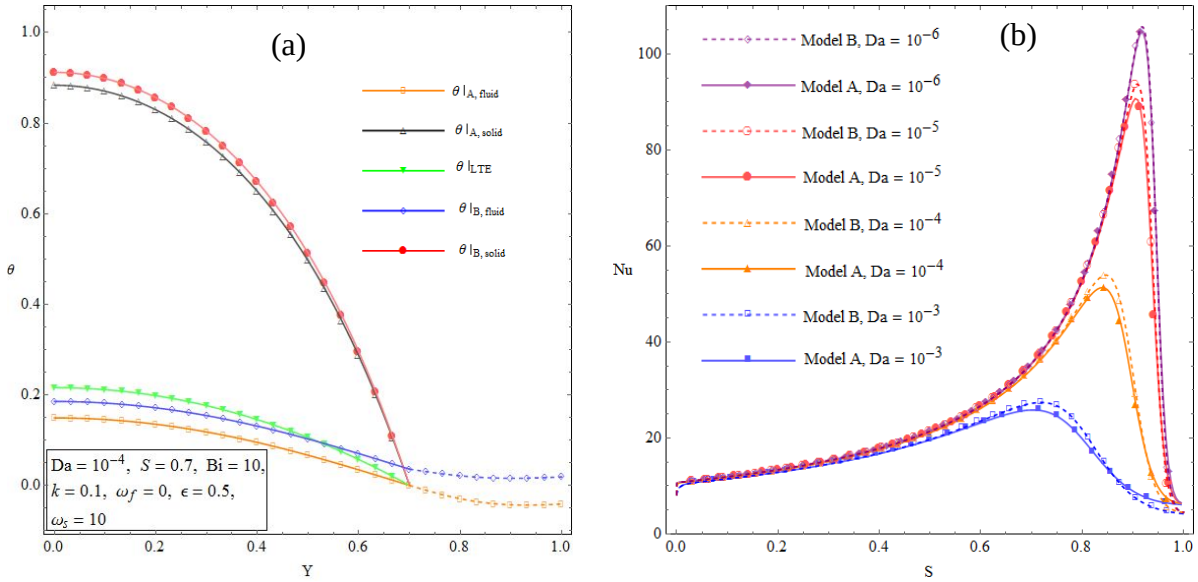

Fig. 2. Comparison between the current results with the literature for $\phi = 0$, lines: previously published results, symbols: current results, (a) temperature fields for $\omega_{nf} = 0, \omega_s = 10$ [40] and (b) Nusselt number for $\omega_{nf} = \omega_s = 0$ [50].

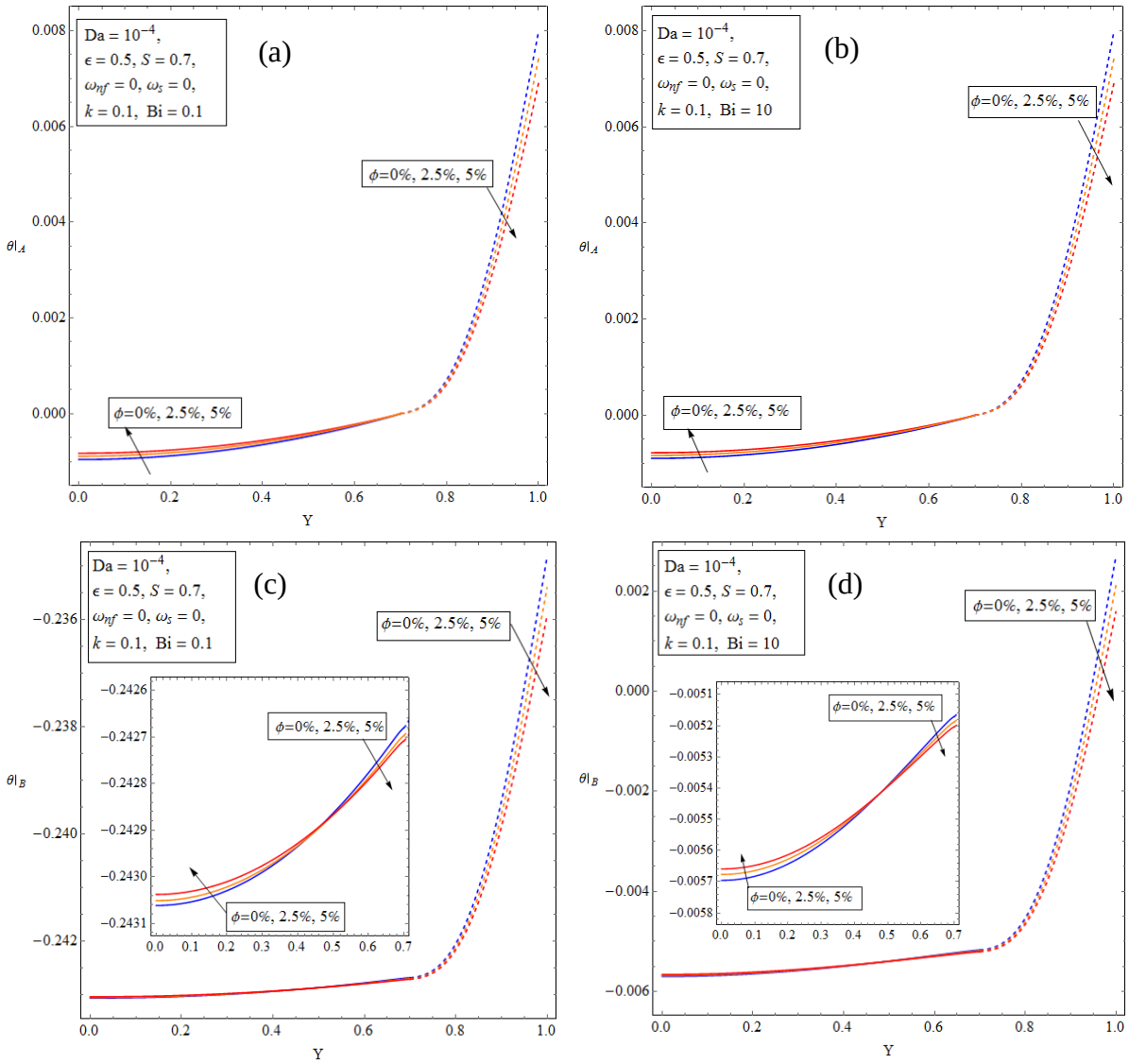

Fig. 3. Dimensionless, nanofluid temperature distribution for Models A and B under varying *Bi* and nanoparticles concentration, k=0.1 and non-heat generating case ($\omega_{nf} = \omega_s = 0$).

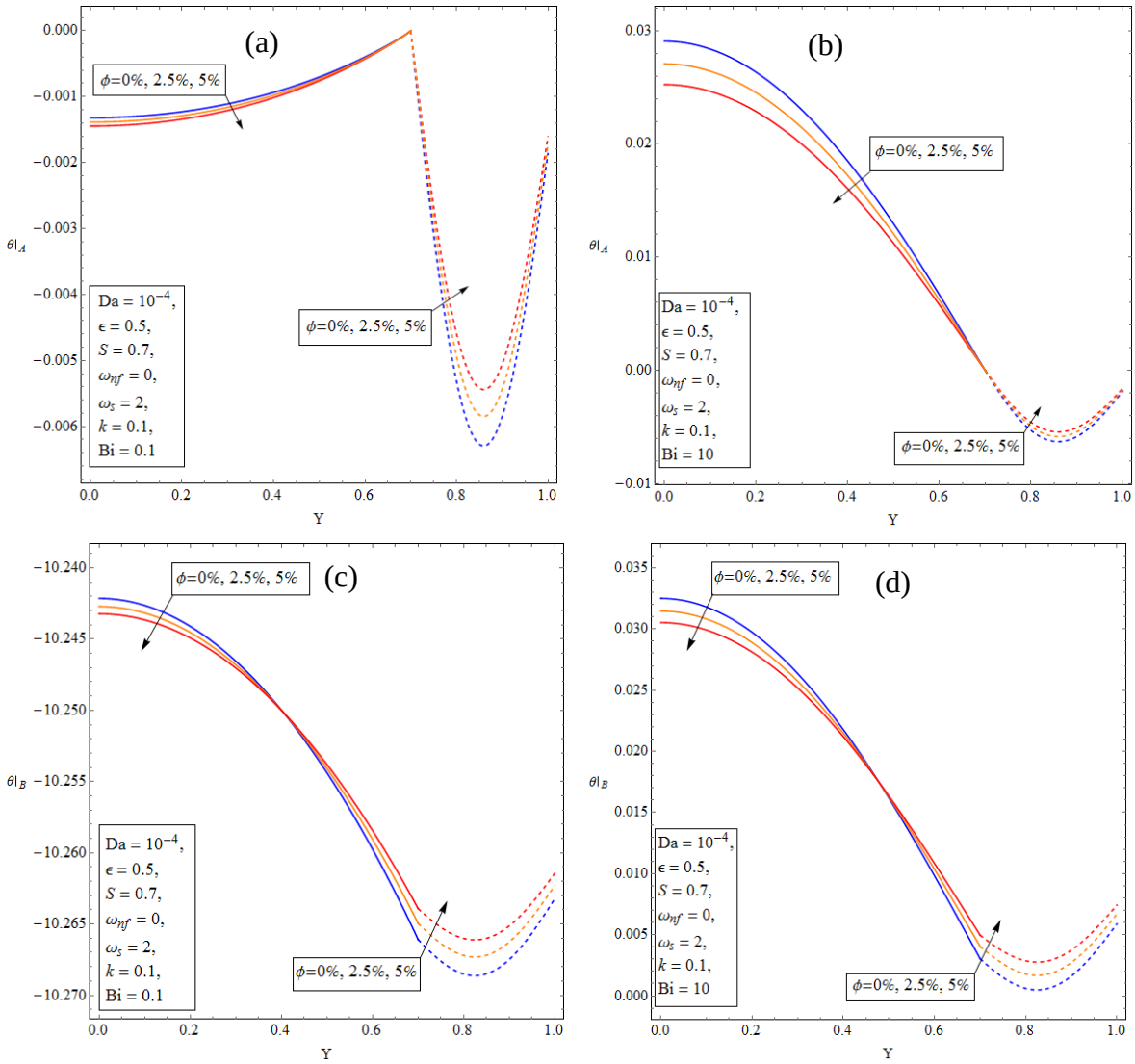

Fig. 4. Dimensionless nanofluid temperature distribution for Models A and B under varying *Bi* and nanoparticles concentration, k=0.1 and solid heat generating case ($\omega_{nf} = 0, \omega_s = 2$).

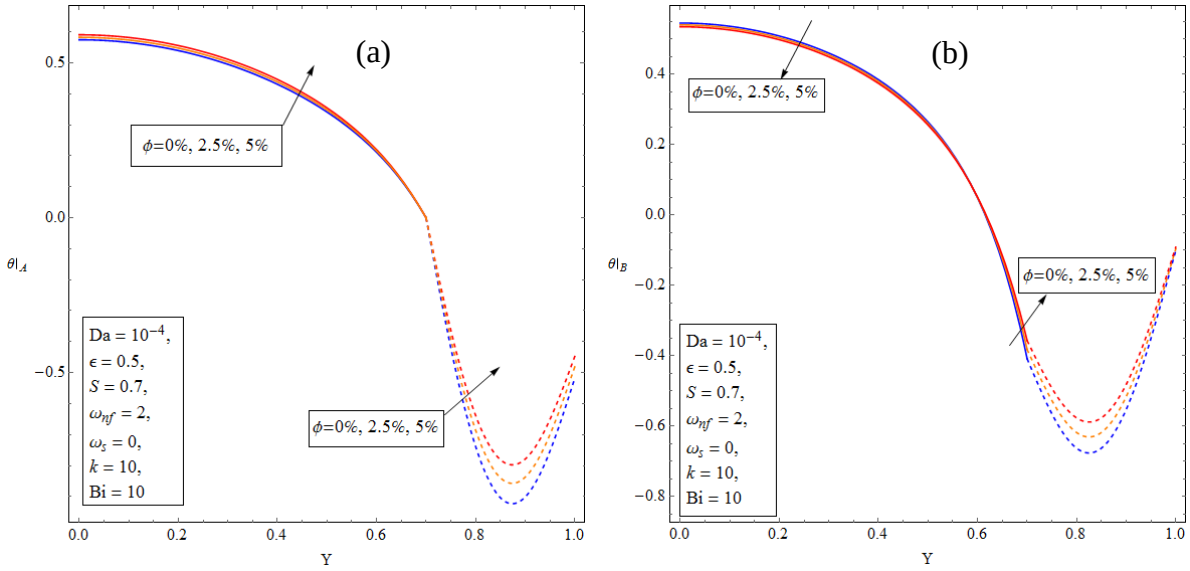

Fig. 5. Dimensionless nanofluid phase temperature distribution for Models A and B and under different values of nanoparticles concentration, ($\omega_{nf} = 2, \omega_s = 0$).

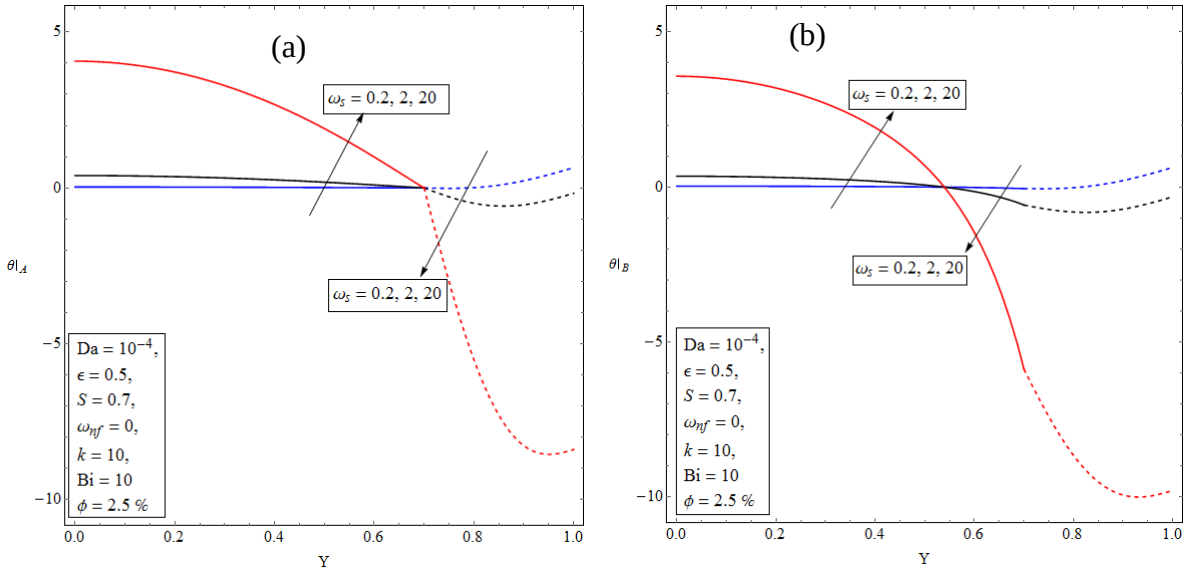

Fig. 6. Dimensionless nanofluid phase temperature distribution for Models A and B and different values of internal heat generation in solid media ($\omega_{nf} = 0, \omega_s = 2$).

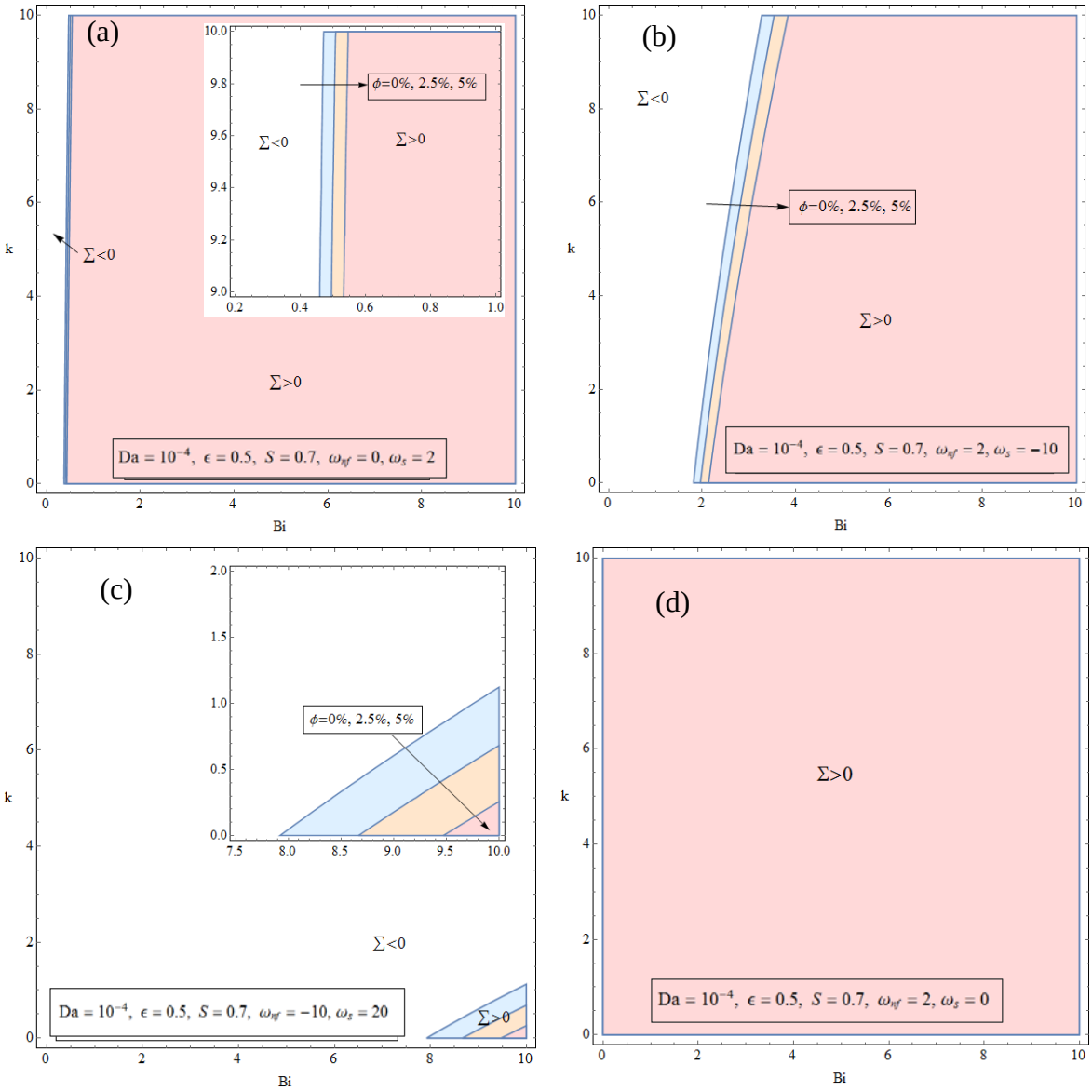

Fig 7. Heat flux bifurcation at the porous interface using various combinations of internal heat generation.

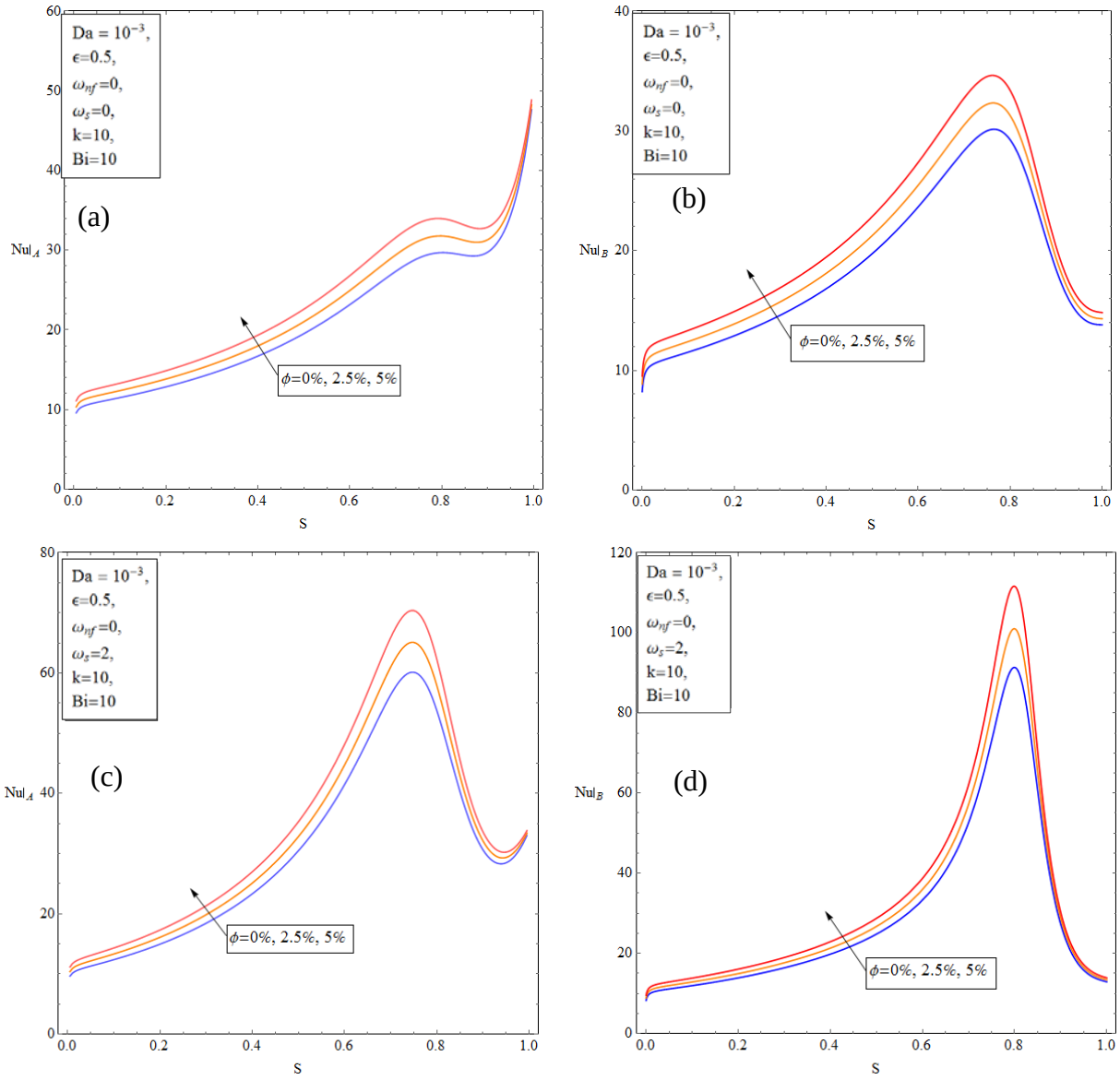

Fig. 8. Nusselt number for Models A and B versus the porous thickness for different values for nanoparticles concentration, (a) & (b): $\omega_{nf} = 0, \omega_s = 0$, (c) & (d): $\omega_{nf} = 0, \omega_s = 2$.

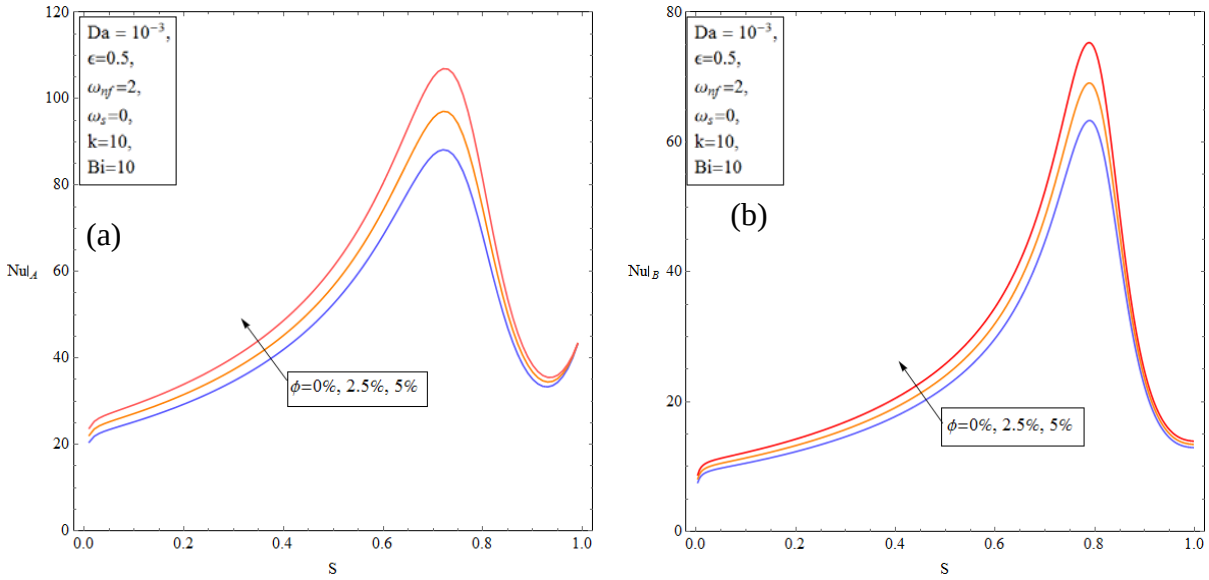

Fig. 9. Nusselt number for Models A and B and varying porous thickness and values for nanoparticles concentration rate, ($\omega_{nf} = 2, \omega_s = 0$).

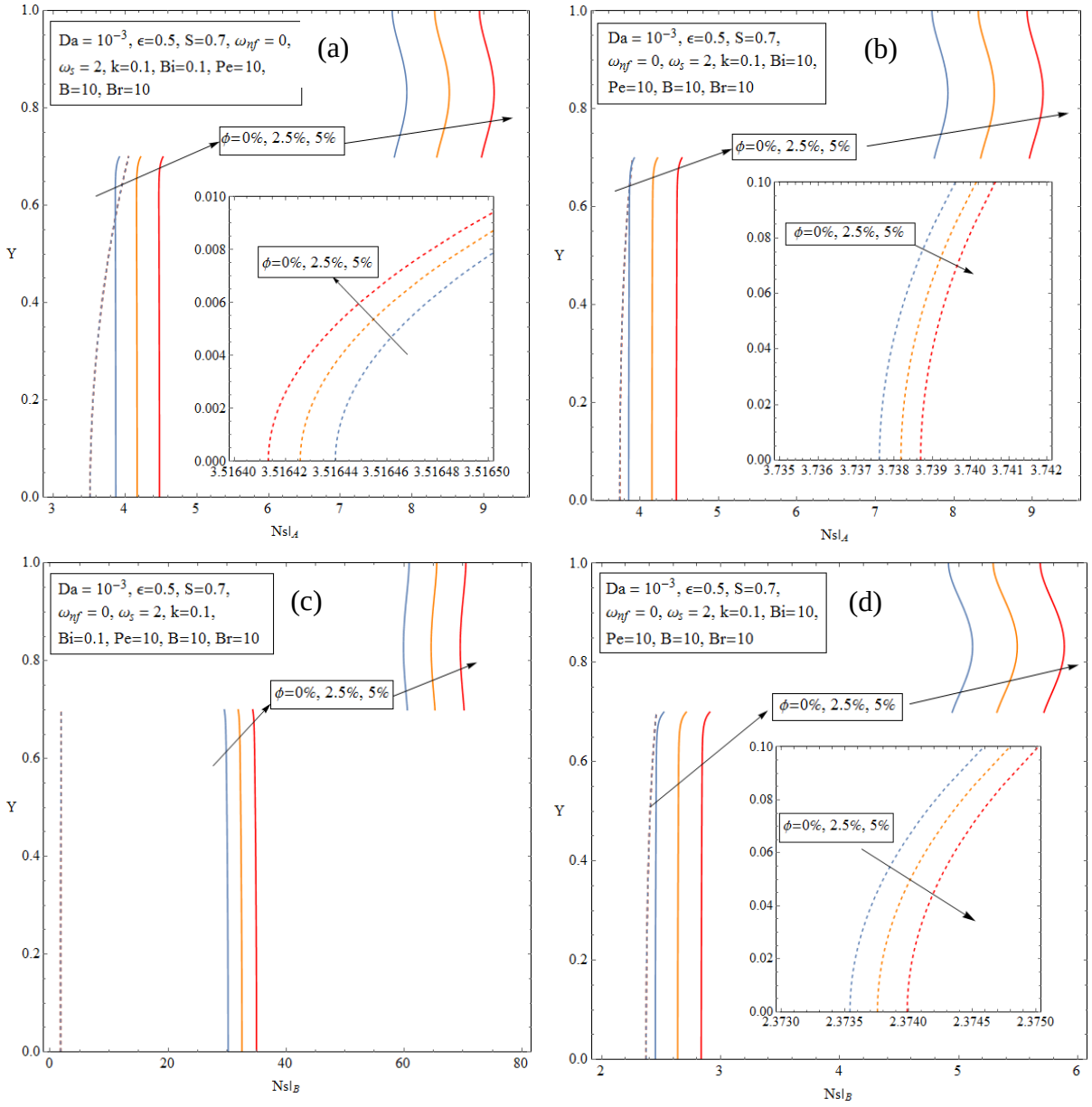

Fig. 10. Dimensionless local entropy generation rate for Models A and B and varying values of *Bi* and nanoparticles concentration, k=0.1 ($\omega_{nf} = 0, \omega_s = 2$) (dash line: solid phase, solid line: nanofluid phase).

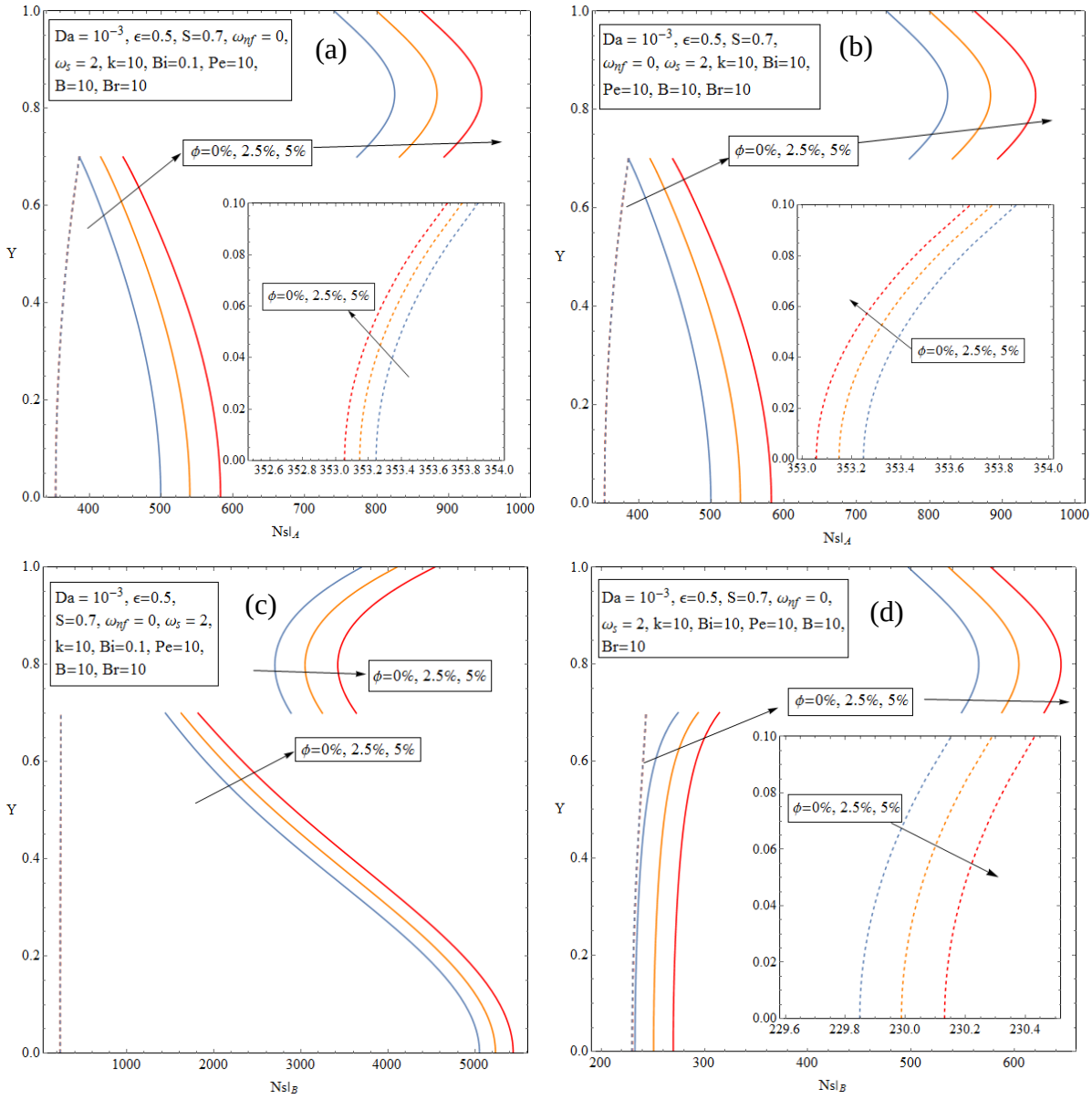

Fig. 11. Dimensionless local entropy generation rate for models A and B and varying values *Bi* and nanoparticles concentration, k=10 ($\omega_{nf} = 0, \omega_s = 2$) (dash line: solid phase, solid line: nanofluid phase).

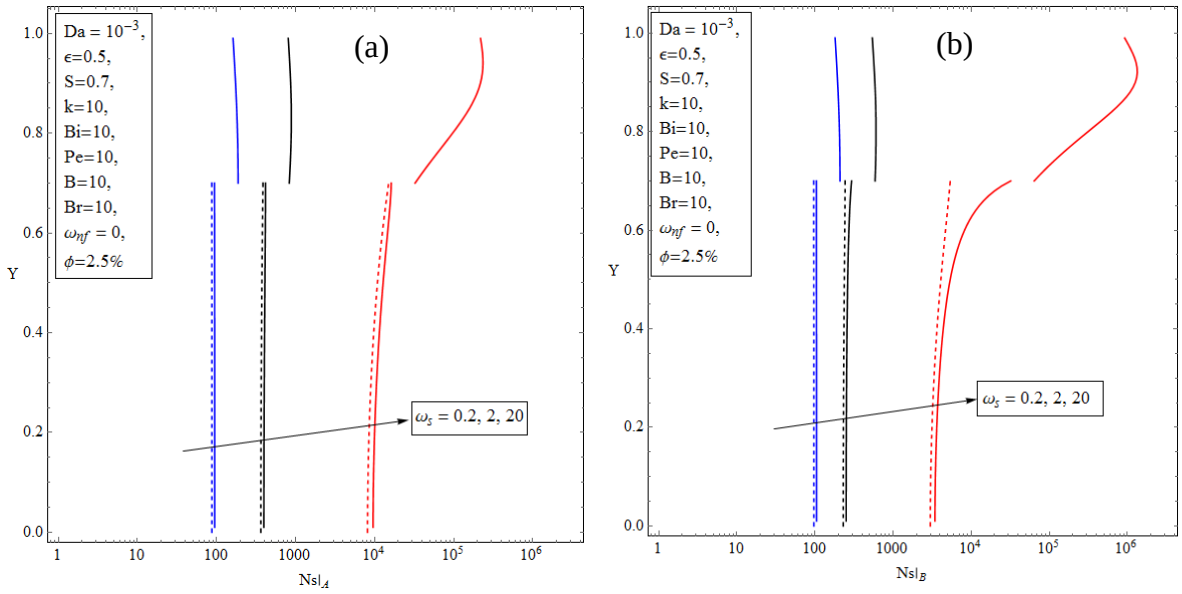

Fig. 12. Dimensionless local entropy generation rate for both models and different values of internal heat generation in the solid medium (dash line: solid phase, solid line: nanofluid phase).

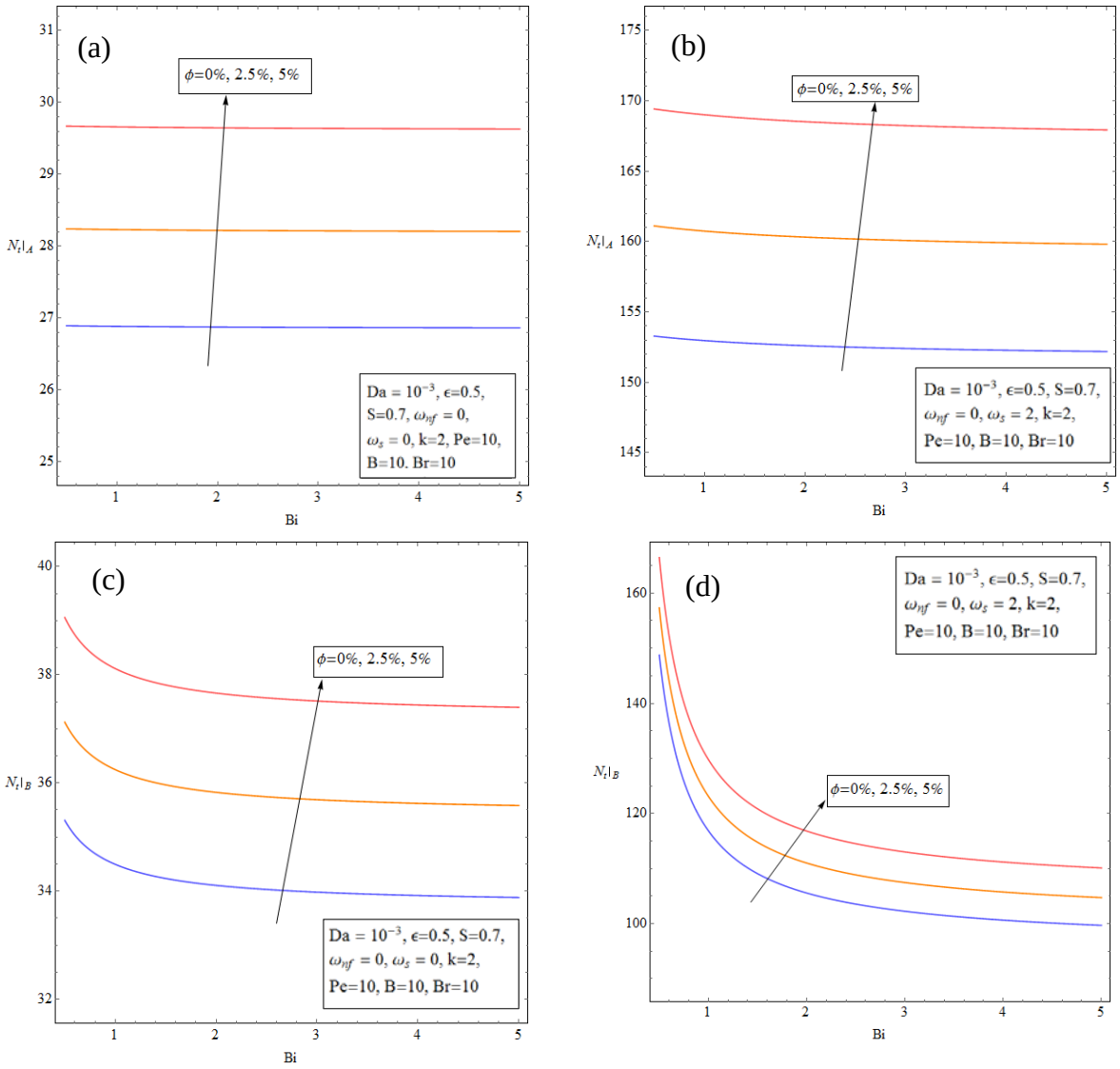

Fig. 13. Total entropy generation rate for Models A and B versus *Bi* and different values for nanoparticles concentration, (a) & (c): $\omega_{nf} = 0, \omega_s = 0$, (b) & (d): $\omega_{nf} = 0, \omega_s = 2$.

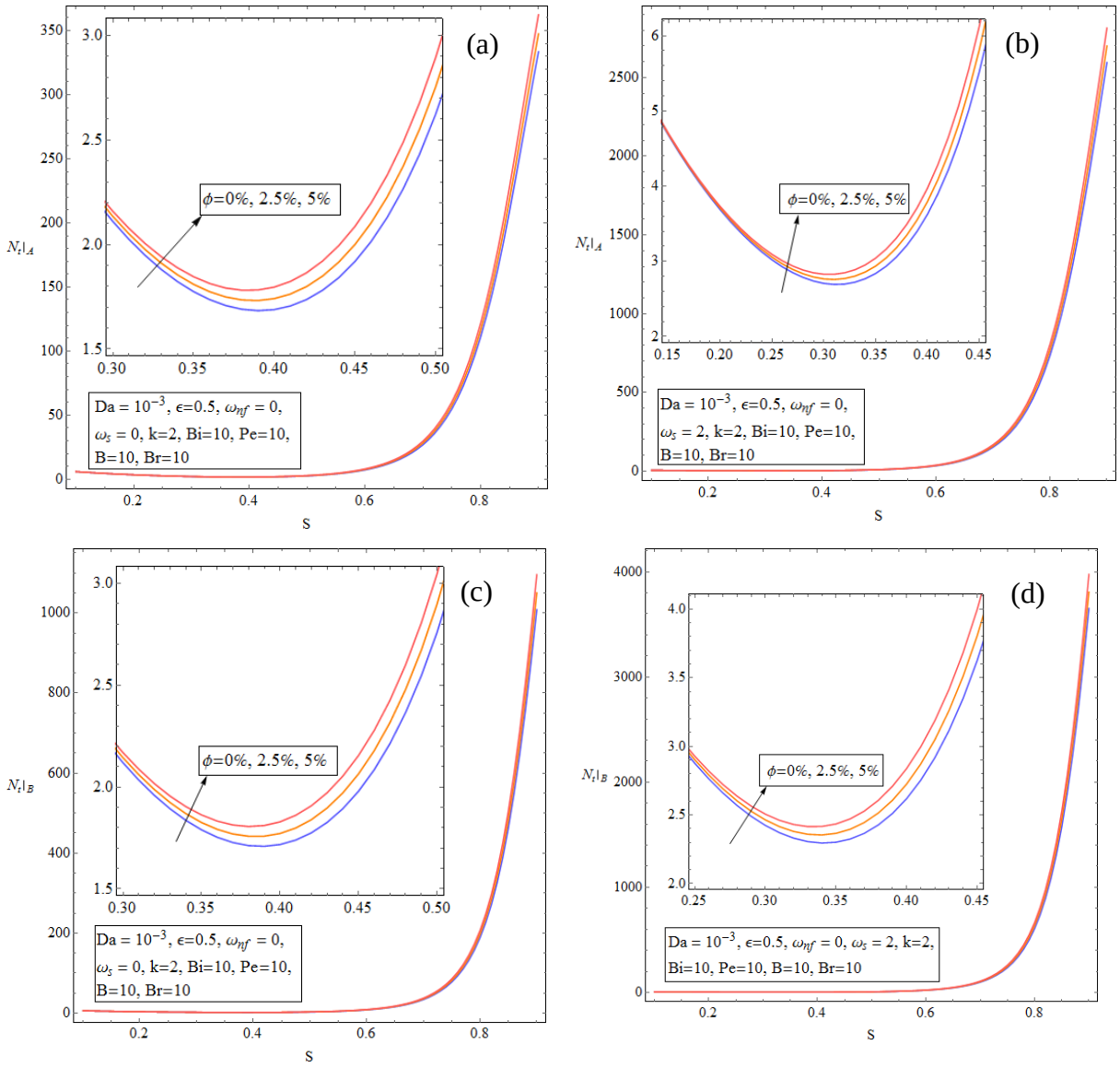

Fig. 14. Total entropy generation rate Models A and B versus the porous thickness for different values of nanoparticles concentration, (a) & (c): $\omega_{nf} = 0, \omega_s = 0$, (b) & (d): $\omega_{nf} = 0, \omega_s = 2$.

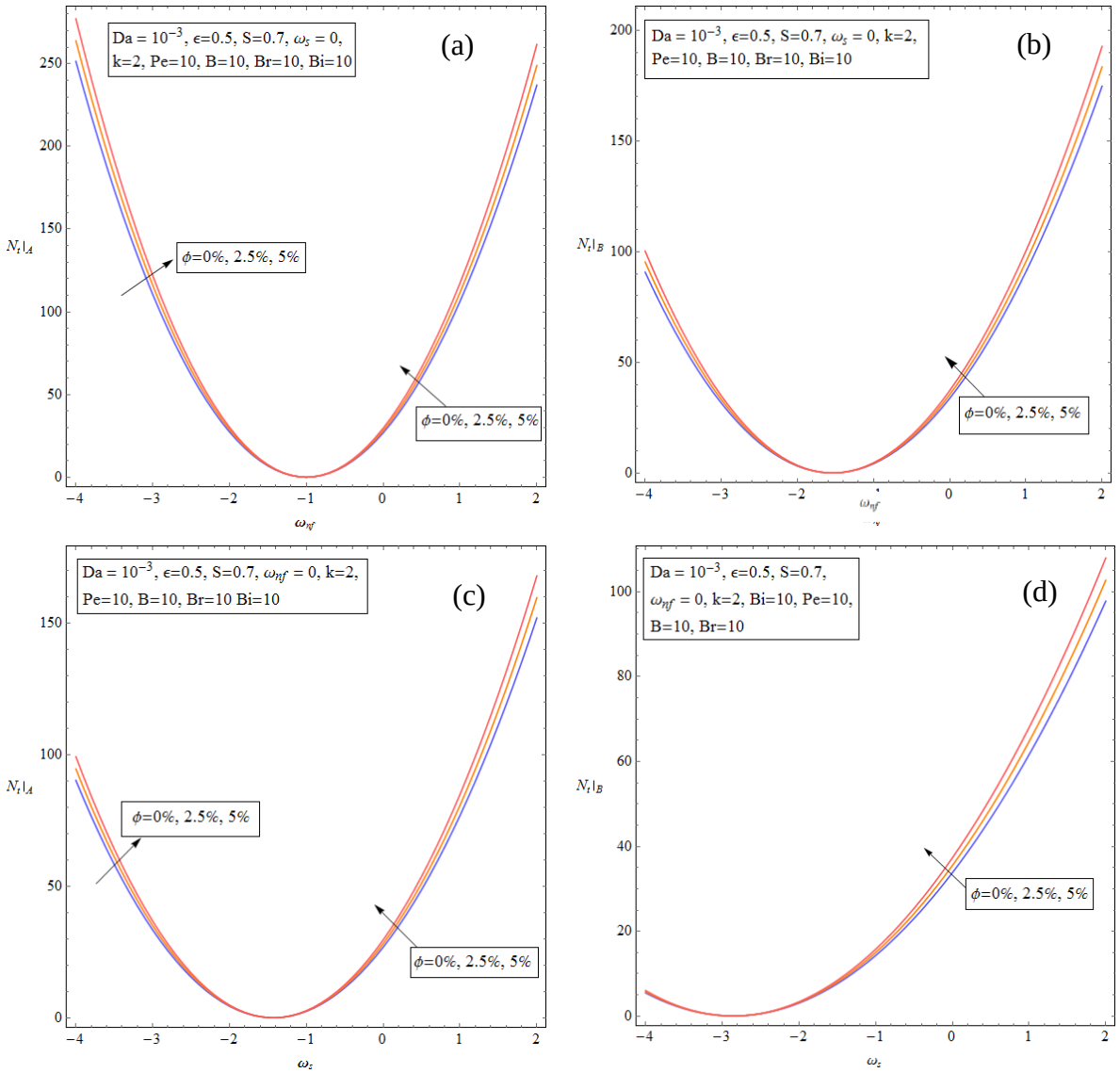

Fig. 15. Total entropy generation rate for Models A and B versus internal heat generations under different values of nanoparticles concentration.

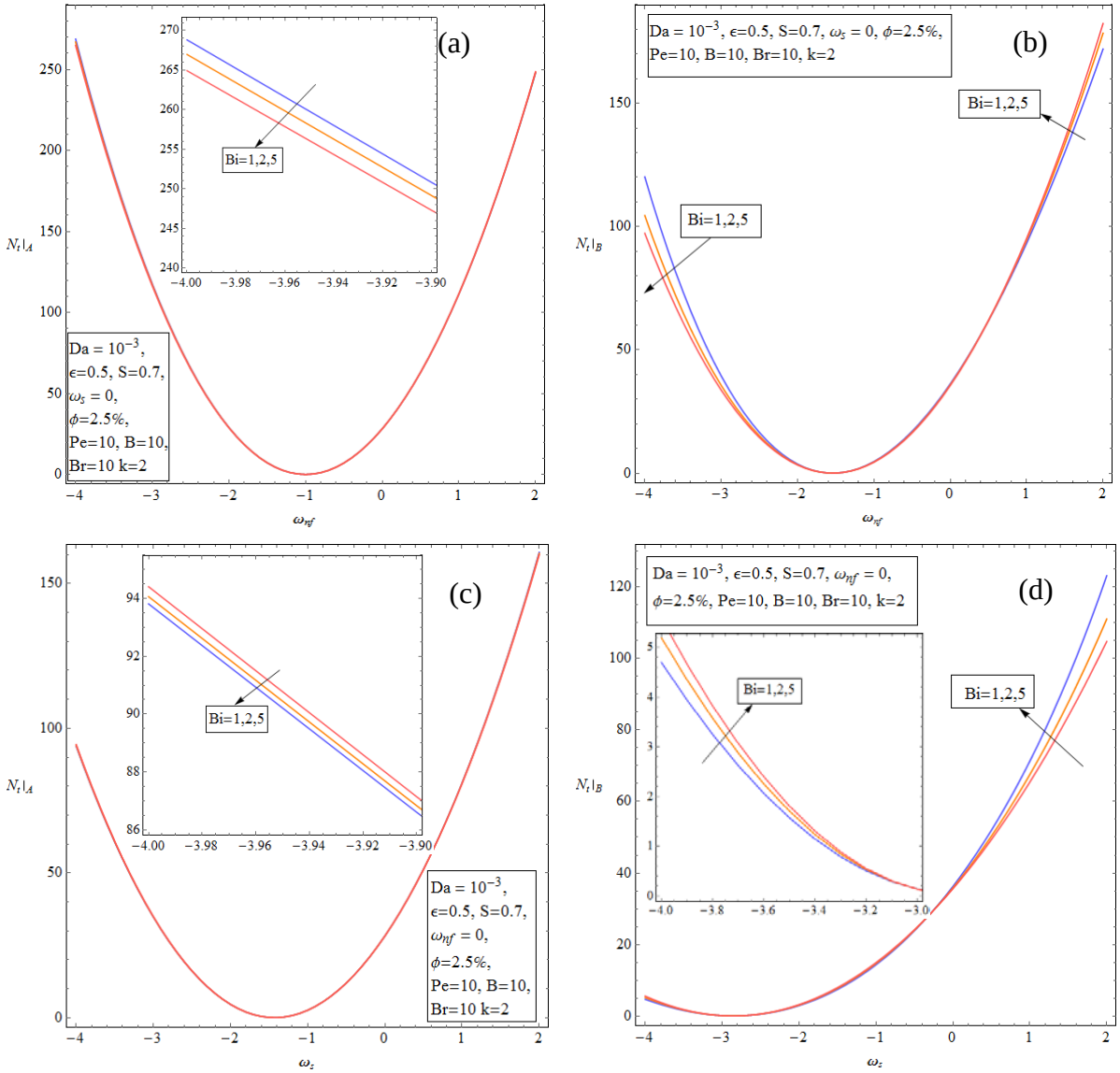

Fig. 16. Total entropy generation rate for Models A and B versus internal heat generations under different values of Biot number.

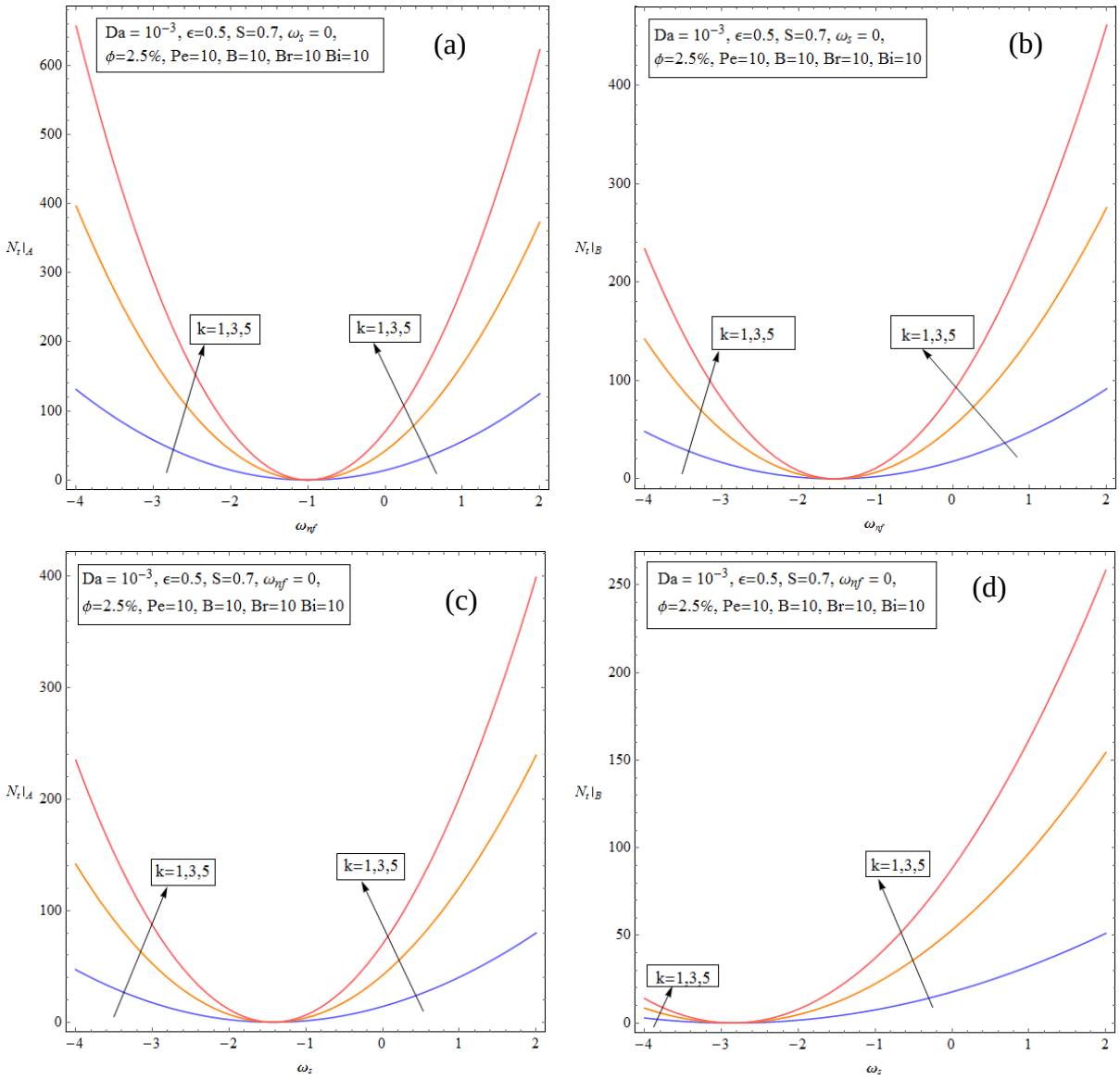

Fig. 17. Total entropy generation rate for Models A and B versus internal heat generations under different values of thermal conductivity ratio.

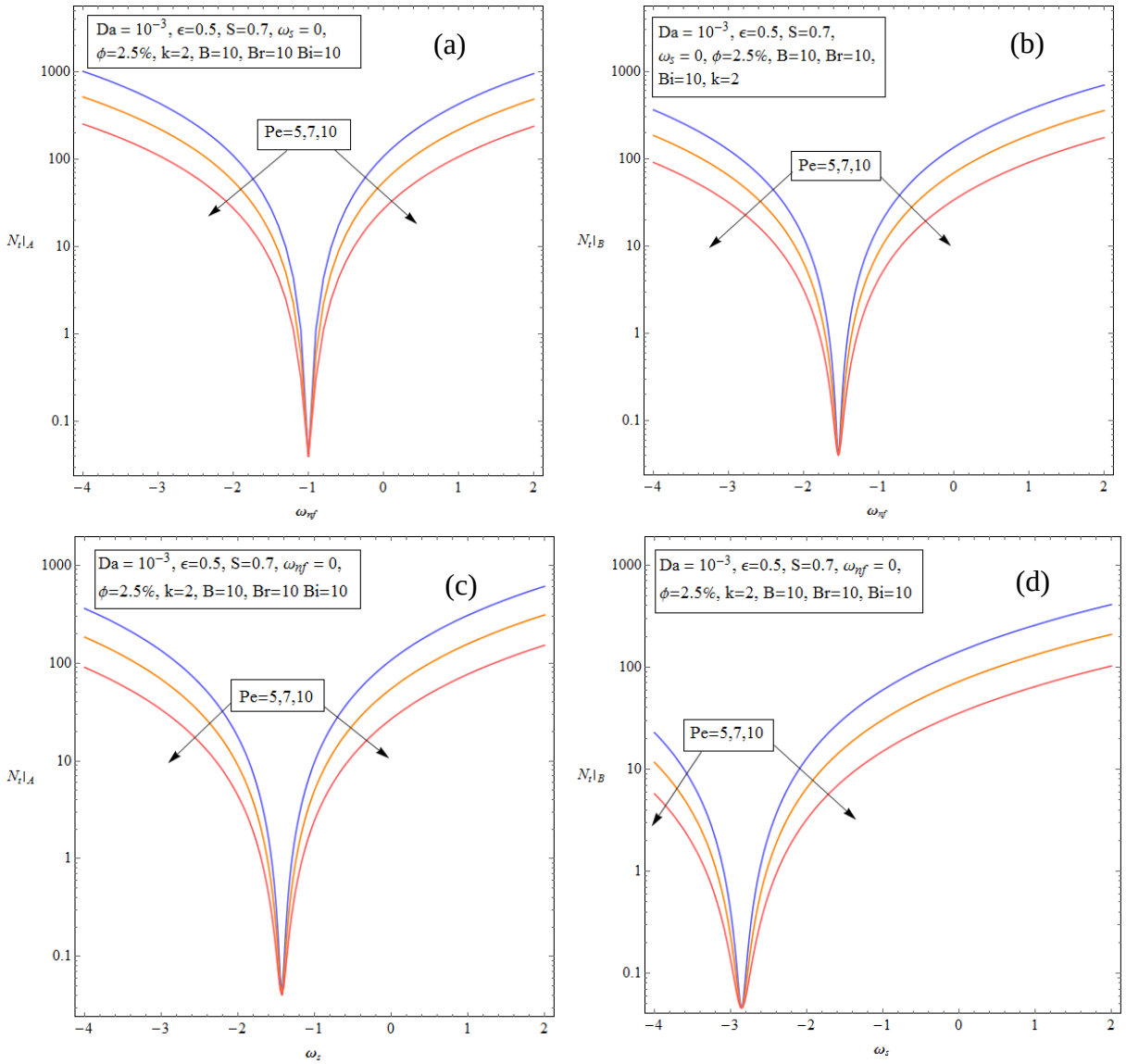

Fig. 18. Total entropy generation rate for Models A and B versus internal heat generations under different values of Peclet number.